bioRxiv preprint doi: https://doi.org/10.1101/2025.01.21.634043; this version posted January 25, 2025. The copyright holder for this preprint (which was not certified by peer review) is the author/funder, who has granted bioRxiv a license to display the preprint in perpetuity. It is made available under a CC-BY 4.0 International license.

REVIEW COMMONS MANUSCRIPT

IMPORTANT:

- Manuscripts submitted to Review Commons are peer reviewed in a journal-agnostic way.
- Upon transfer of the peer reviewed preprint to a journal, the referee reports will be available in full to the handling editor.
- The identity of the referees will NOT be communicated to the authors unless the reviewers choose to sign their report.
- The identity of the referee will be confidentially disclosed to any affiliate journals to which the manuscript is transferred.

GUIDELINES:

- For reviewers: https://www.reviewcommons.org/reviewers
- For authors: https://www.reviewcommons.org/authors

CONTACT:

The Review Commons office can be contacted directly at: office@reviewcommons.org

bioRxiv preprint doi: https://doi.org/10.1101/2025.01.21.634043; this version posted January 25, 2025. The copyright holder for this preprint (which was not certified by peer review) is the author/funder, who has granted bioRxiv a license to display the preprint in perpetuity. It is made available under a CC-BY 4.0 International license.

Protein Kinase C positively regulates peroxisome biogenesis by promoting peroxisome-endoplasmic reticulum interaction

Anya Borisyuk[1], Charlotte Howman[2], Sundararaghavan Pattabiraman[3], Daniel Kaganovich[2,4], Triana Amen[1,2]

[1.] Global Health Institute, Faculty of Life Sciences, Ecole Polytechnique Fédérale de Lausanne, Lausanne, Switzerland

[2.] School of Biological Sciences, University of Southampton, Southampton, UK

[3.] 1BasePharma, Israel

[4.] 2Prime Ltd, UK

Short title: Protein Kinase C induces peroxisome proliferation

Keywords:
Peroxisome, Protein Kinase C, GSK3β, PEX11b, VAPB, contact sites, peroxisome biogenesis, peroxisome division, signaling

Correspondence: t.amen@soton.ac.uk, d.kaganovich@soton.ac.uk

bioRxiv preprint doi: https://doi.org/10.1101/2025.01.21.634043; this version posted January 25, 2025. The copyright holder for this preprint (which was not certified by peer review) is the author/funder, who has granted bioRxiv a license to display the preprint in perpetuity. It is made available under a CC-BY 4.0 International license.

Abstract

Peroxisomes carry out a diverse set of metabolic functions, including oxidation of very long-chained fatty acids, degradation of D-amino acids and hydrogen peroxide, and bile acid production. Many of these functions are upregulated on demand, therefore cells control peroxisome abundance, and by extension peroxisome function, in response to environmental and developmental cues. The mechanisms upregulating peroxisomes in mammalian cells have remained unclear. Here we identify a signaling regulatory network and a mechanism that coordinate cellular demand for peroxisomes and peroxisome abundance by regulating peroxisome proliferation. We show that protein kinase C (PKC) promotes peroxisome PEX11b-dependent formation. PKC activation leads to an increase in peroxisome formation, promoting peroxisome-ER contact site formation through inactivation of GSK3β. We show that removal of VAPA and VAPB impairs peroxisome biogenesis and PKC regulation. Inhibition of PKC reduces peroxisome-ER interactions, leading to a decrease in peroxisome abundance. During neuronal differentiation, active PKC leads to a significant increase in peroxisome formation. We propose that peroxisomal regulation by transient active PKC signaling enables rapid and fine-tuned responses to the need for peroxisomal activity.

Introduction

The peroxisome is a small organelle with a large functional repertoire [1-3]. Prominent examples of peroxisomal function are alpha- and beta-fatty acid oxidation, bile acid and ether-lipid synthesis, degradation of D-amino acids and leukotrienes, glyoxylate cycle and methanol metabolism in yeast, bioluminescence in fireflies, plant hormone synthesis, and degradation of hydrogen peroxide [2-15]. In addition to their numerous metabolic functions, peroxisomes are increasingly seen as signaling regulators [16-20]. Several kinases, (e.g. the NDR2 kinase regulator of ciliogenesis) contain peroxisome localization signals [21, 22]. The peroxisomal membrane has been shown to recruit multiple signaling regulators, including the tuberous sclerosis complex (TSC1/2) regulator of the target of rapamycin (mTOR) kinase pathway, which binds to peroxisomal proteins PEX19 and PEX5 [16-20].

Due to the diversity of peroxisomal functions, the cellular demand for peroxisomes depends on specific conditions, such that peroxisomes must be rapidly mass-produced during specific instances of stress adaptation and development [7, 23, 24], necessitating precise regulation. Disruption of peroxisomal biogenesis adversely affects downstream cellular adaptive functions, including autophagy, cholesterol metabolism, immune response, and ciliogenesis [20, 22, 25-29]. Not surprisingly, therefore, multiple human disorders result from defects in peroxisome biogenesis [2, 30-32]. Due to the transient “on demand” need for peroxisomal metabolism, the key to understanding the role of peroxisomes in cell biology and disease is to investigate the mechanisms regulating peroxisomal biogenesis.

Peroxisomes form through two main pathways: fission of pre-existing peroxisomes [33-38], and *de novo* (from intracellular endoplasmic reticulum- and mitochondria-derived membranes) [35, 36, 39-44]. The peroxisome biogenesis machinery consists of peroxins (PEX), which are conserved in fungi, plants, and animals [34, 45-48]. Deletion of PEX3, PEX19 and PEX16 results in conditionally viable cells lacking peroxisomes [34, 39, 41, 43, 44, 47, 49-52]. Peroxisome division, on the other hand, is initiated by the PEX11 protein family, which orchestrate a multistep process that involves peroxisome membrane elongation, and prime assembly of additional peroxisome division components, including MFF, FIS1, and DNM1L 53-57. Both peroxisome biogenesis mechanisms are initiated by several non-mutually exclusive pathways: transcriptional peroxisome proliferator receptor alpha (PPARα) increases the level of division factors, peroxisome tethering to the endoplasmic reticulum (ER) through a recently defined membrane contact site that is formed between acyl-coenzyme A-binding domain protein 5 (ACBD5) and the ER protein vesicle-associated membrane protein-associated protein (VAPB)[58, 59] potentially sources the membrane, and an increase in peroxisome function in the presence of peroxisomal substrates promotes peroxisome formation via unknown mechanissms. The latter phenomenon of increased peroxisome number in response to increased peroxisomal function is known as “metabolic control of peroxisome abundance (MCPA)” [23, 60-63]. Recently, Schrader/Costello groups demonstrated how peroxisome-endoplasmic reticulum membrane contacts are negatively regulated by glycogen synthase kinase beta (GSK3β) that phosphorylates ACBD5 preventing interaction with

bioRxiv preprint doi: https://doi.org/10.1101/2025.01.21.634043; this version posted January 25, 2025. The copyright holder for this preprint (which was not certified by peer review) is the author/funder, who has granted bioRxiv a license to display the preprint in perpetuity. It is made available under a CC-BY 4.0 International license.

VAPB and reducing contacts[58, 64, 65]. We showed that abolishing the peroxisome-ER contacts through knockout of VAPB and its homologue VAPA leads to a significant defect in peroxisome biogenesis[66].

Here, using a focused tool compound kinase inhibitor screen, we identify positive and negative regulators of peroxisome abundance, including PKC as a major positive driver. We show that active PKC inhibits GSK3β, promoting peroxisome-ER tethering and peroxisome biogenesis, promoting ACBD5-VAPB interaction[58, 67, 68]. We further show that PKC regulation is dependeend on PEX11b and VAPs. Inhibition of PKC reduces peroxisome-ER contacts, peroxisome abundance, and function. Our study shows how PKC can rapidly regulate peroxisome-ER interaction, peroxisome formation, and peroxisome function.

Results:

Tool Compound Kinase Inhibitor screen reveals signaling regulators of peroxisome abundance

We postulated that a sensitive and tractable assay of peroxisome abundance was the key to discovering regulators of peroxisome formation and, by extension, peroxisome function. We therefore developed a new tool for quantifying peroxisomes in live cells. We used CRISPR/Cas9 gene editing to genomically fuse GFP to the C-terminus of the transmembrane peroxisomal protein PMP70 in HEK293T cells (Figure 1A; Figure S1A and S1B). PMP70-GFP localized to peroxisomes, peroxisomal protein import was not impaired, and peroxisomes in the endogenously tagged cells were comparable to the wildtype cells (Figure S1C, S1D, and S1E). Considering the prominent role of kinase signaling in metabolic regulation, we set out to identify kinase modulators of peroxisome abundance. We opted for a small molecule "tool compound" library of 152 kinase inhibitors, which we viewed as preferable to gene manipulation-based screening given the pleiotropic and essential nature of regulatory kinase function (Figure 1B; Figure S1F, Figure S2, Figure S3, and Supplementary Table 1). Peroxisome cellular density (abundance) was calculated as the number of peroxisomes per square micron of the cytoplasmic space in confocal microscopy images, using the overexpression of PEX19 peroxisome biogenesis factor as a positive control[49], and overexpression of PEX3 as a negative control (Figure 1C) [69, 70]. We found that 16 kinase inhibitors reduced, and 5 upregulated, the number of peroxisomes in HEK293T cells (Figure S1F and S1G). We performed a secondary screen of the hits in untagged human fibroblasts (Figure 1D), validating 10 compounds that reduced and 2 that upregulated the number of peroxisomes (Figure 1E). We then associated the molecules to the kinases they inhibit and mapped the kinases on the human kinome (Figure 1F). Positive regulators (whereby inhibition of the kinase reduces peroxisome number) included: protein kinase C (PKC), TGFβR, MEK1/2, ERK2, PDHK, IGF1R, and ALK4/7. Negative regulators (whereby inhibition of the kinase increases peroxisome numbers) were CK2 and IKKβ (Figure 1F). Two different tool compounds targeted the TGFβ and PKC pathways. Interestingly, TGFβ is a known positive regulator of peroxisome proliferation [71], underlining the broad coverage of our tool compound screen. We elected to further focus on the previously uncharacterized role of PKC in regulating peroxisome abundance.

Protein Kinase C delta positively regulates peroxisome abundance

First, we analyzed which PKC isoforms are inhibited by the small molecules that we identified. Go6983 PKC inhibitor prevents kinase activity as well as the steric PKC interaction with the substrates [72]. Chelerythrine and D-erythrosphingosine C18 are potent inhibitors of PKC[73, 74]. The human PKC superfamily consists of classical (cPKC): α, βI, βII, γ; novel (nPKC): δ, ε, θ and η: atypical (aPKC): ζ and ι / λ: and PKC-related kinase (PKN) isoforms [75, 76]. Identified molecules are not specific to one isoform, and inhibit classical (cPKC: α, β. and γ), novel (nPKC δ), and at least one atypical (aPKC : ζ), inhibition of these PKC isoforms resulted in a decrease of peroxisome abundance (Figure 1E). We, therefore decided to test whether PKC activation by overexpression of one isoform is sufficient to trigger peroxisome proliferation. First, we overexpressed a representative isoform of each class - classical PKC(α), novel PKC(δ), and atypical isoform of PKC(ζ) fused to mCherry and mCherry as a control and measured peroxisome number (Figure 2A-B). Only PKCδ overexpression was able to induce peroxisome proliferation (Figure 2A; Figure S4A). Both cPKC and nPKC bind to and are activated by phorbol esters (PMA)[77, 78]. We incubated human fibroblasts with PMA, which

bioRxiv preprint doi: https://doi.org/10.1101/2025.01.21.634043; this version posted January 25, 2025. The copyright holder for this preprint (which was not certified by peer review) is the author/funder, who has granted bioRxiv a license to display the preprint in perpetuity. It is made available under a CC-BY 4.0 International license.

resulted in a significant increase in peroxisome number (Figure 2C). Together, these data argue that PKCδ is a positive regulator of peroxisome abundance in human cells. To independently test that inhibition of PKC affects peroxisome biogenesis we used a radioactive assay of peroxisomal fatty acid oxidation that we previously established[66]. As a control we generated PEX19 KO that lack peroxisomes (Figure 2D)[66]. Inhibition of PKC resulted in a significant reduction of peroxisome function, but did not inhibit it completely (Figure 2D), consistent with a reduction of peroxisome numbers. PKC, therefore, regulates peroxisome biogenesis – formation and function of peroxisomes. Next, investigated the mechanism of this new role of PKC in peroxisome biology.

Protein Kinase C induces PEX11b-dependent peroxisome formation

Peroxisome abundance is maintained by peroxisome biogenesis by *de novo* and division pathways, and peroxisome degradation [35, 39, 43, 45, 53, 79-82]. To understand how PKC activation results in an increased number of peroxisomes, we first reproduced the PEX19 functional complementation assay [41] in HEK293T cells (Figure 3A). This assay monitors *de novo* peroxisome formation by complementing PEX19 KO cells with PEX19 and measuring peroxisome formation. We constructed CRISPR/Cas9 PEX19 KO cells, that lack peroxisomes[66]. In line with published observations, it takes more than 24 hours to restore peroxisomes *de novo* [36, 41] (Figure 3B). Peroxisomes appear on the second day after transfection and continue to proliferate, with a 70% restoration on day 4 (Figure 3B-D). PKC inhibition did not change the *de novo* peroxisome formation. Note, that here we measured the ratio of cells that restored peroxisomes among the cells expressing PEX19 (the density of peroxisomes in single cells was not assayed). Similarly, PKC activation with PMA did not affect *de novo* peroxisome formation, however, a long exposure to PMA is inhibitory to PKC, as active PKC is degraded [83]. Peroxisome division is thought to be a more frequent event than peroxisome *de novo* formation [84], and it takes considerably less time. Peroxisome proliferation was upregulated with a short 2-hour exposure to PMA that activates PKC, pointing towards the proliferation pathway as a point of PKC regulation of peroxisome abundance (Figure 3E).

Peroxisome proliferation is controlled by PEX11b - a key peroxisomal proliferation factor, responsible for early membrane remodeling, elongation, and association with the rest of the division machinery that is shared with mitochondria [38, 53, 54]. In order to understand whether PKC regulates PEX11b-induced peroxisome division we constructed a CRISPR/Cas9 PEX11b KO (Figure 3F). PEX11b KO has a reduction in peroxisome abundance as was previously shown, and it did not respond to PKC inhibition by further reduction of peroxisome numbers (Figure 3G and 3H) [54, 85].

Finally, to rule out PKC-driven regulation of the PPARα peroxisomal transcriptional regulator [86], we measured PPARα levels following PKC inhibition and activation. PKC inhibition had no effect on PPARα, whereas PKC activation with PMA showed a modest increase in PPARα levels, though not PPARα activity (Figure S4B-E)[87, 88]. To also rule out a role for pexophagy [89], we silenced the NBR1 receptor, which did not affect peroxisome abundance over a two day period (Figure S4F, S4G), confirming that PKC does not upregulate peroxisomes by inhibiting their degradation. Collectively these data points to the peroxisome division pathways as a route for PKC regulation of peroxisome abundance. Next, we investigated the mechanism of PKC regulation of peroxisome proliferation.

PKC phosphorylation of PEX11b on S53 is not sufficient to induce peroxisome proliferation

First, to explore whether PEX11b machinery is reorganized during PKC inhibition, we tested whether PEX11b changes its association with other division factors. However, neither the interaction of PEX11b with other factors of peroxisome division machinery or PEX19 (Figure 3I-J) were significantly affected.

PEX11 phosphorylation is known to promote peroxisome division in certain yeast species (*Saccharomyces cerevisiae* and *Pichia pastoris)*, but not in others (*H. polymorpha)* [90-92]. Therefore, we were curious whether phosphorylation of PEX11b by PKC regulates proliferation of peroxisomes in human cells. There are 6 predicted PKC phospho-sites on PEX11b according to NetPhos3.1 prediction algorithm [93, 94]. Mass spectrometry analysis of the PEX11b in the lysate results in low peptide coverage, not sufficient for the phospho-proteomic identification. To overcome this limitation,

bioRxiv preprint doi: https://doi.org/10.1101/2025.01.21.634043; this version posted January 25, 2025. The copyright holder for this preprint (which was not certified by peer review) is the author/funder, who has granted bioRxiv a license to display the preprint in perpetuity. It is made available under a CC BY 4.0 International license.

we constructed a CRISPR/Cas9 flag-GFP-PEX11b HEK293T cell line (Figure S5A). Flag pull-down of PEX11b significantly improved PEX11b coverage (Figure S6A), and was used for targeted phospho-peptide identification (Figure S5B, Supplementary Table 2). Among the identified peptides, Ser53 is a predicted PKC target, Ser38 is an unspecified/p38MAPK target, and Ser78 was not identified by the prediction algorithm (Figure S5B; Figure S6B-C). The ratio of phosphorylated to the overall identified peptides was 4.4% for Ser53. To confirm that PKC can directly phosphorylate Ser53 of PEX11b we used a pure peptide competition assay – a mix of all the predicted PKC-phosphorylated PEX11b peptides with a known PKC substrate peptide [95], incubated with or without the addition of pure active PKC and subjected to phospho-mass spectrometry (Figure S5B). 4 out of 6 predicted peptides were phosphorylated to a similar extent as the PKC substrate peptide, including the Ser53 site, and none of the peptides were phosphorylated without PKC (Figure S5B-C, S6D).

We overexpressed PEX11b, PEX11b S53A (Ser53Ala), and a phosphomimetic PEX11b S53D (Ser53Asp) mutant in PEX11b KO background and assessed peroxisome number (Figure S5C-F). PEX11b S53D overexpression, and that of the WT and S53A, had no effect on peroxisome number (after correction for PEX11b expression level) (Figure S5E). Importantly, N-terminal phosphorylation of PEX11b on S38, was also shown to have no effect on peroxisome division [96]. We also verified that other identified sites (S78, and a triple D mutant) did not affect the number of peroxisomes either (Figure S5G-H).

PKC regulates peroxisome-ER contact sites through GSK3β inhibition

Given that PKC phosphorylation of PEX11b failed to explain its effect on peroxisome proliferation, we posited that the regulation of the peroxisome-ER interaction can affect peroxisome proliferation. This is based on the discovery of the VAPB-ACDB5 contacts[59, 68] and our finding that KO of VAPA and VAPB results in a significant decrease in peroxisome abundance[66]. In addition to acting as a structural anchor, the VAPB-ACBD5 contact site regulates lipid transfer between the ER and peroxisomes. Since peroxisomes do not produce their own phospholipids, this activity may be essential for division-associated membrane growth[58]. To independently confirm that peroxisome-ER contact sites are required for peroxisome biogenesis (i.e. an increase in the number of peroxisomes), we used VAPB/VAPA knockout cells [97]. There was a significant decrease in peroxisome number in the VAP KO cells, which was restored upon complementation with VAPB (Figure 4A, Figure S4H). Peroxisome abundance in VAP KO cells was significantly reduced, and not affected by PKC inhibition (Figure 4B)[66].

We then assessed peroxisome-ER interaction[58, 59]. Inhibition of PKC resulted in a decrease in the VAPB-ACBD5 interaction as evidenced by the co-immunoprecipitation of VAPB (Figure 4C), and resulted in a significant increase in a free-roaming peroxisomes, as evidenced by the lack of peroxisome-ER proximity (Figure 4D), and significant increase in mobility (Figure 4E-F; Supplementary Movies 1-6). One obvious candidate for the mechanism of this regulation was GSK3β, due to its established role in the VAPB-ACBD5 negative regulation[58, 68]. PKC negatively regulates GSK3β [98, 99], which, in turn, negatively regulates peroxisome contact sites with the ER [68]. We therefore hypothesized that PKC drives peroxisome division by modulating contact site formation. We confirmed that PKC activation inhibits GSK3β, whereas inhibition of PKC leads to GSK3β activation, as assayed by measuring GSK3β S9 inhibitory phosphorylation (Figure 4G). Next, to confirm that PKC regulates peroxisome biogenesis through GSK3β inactivation, we constructed a GSK3β S9A constitutively active mutant[100], which suppressed peroxisome proliferation in response to PMA treatment (PKC activation) (Figure 4H and 4I). Finally, analysis of our hits from the small molecule screen, revealed that inhibitor of GSK3β, CHIR99021, increased peroxisome number in HEK293T cells (Figure S1G). Taken together, these data shows that PKC can positively regulate peroxisome number through inhibition of GSK3β, by promoting peroxisome-ER interaction through known mechanisms[58, 68], which in turn is regulating peroxisome biogenesis (Figure 4A)[66].

Protein kinase C regulates peroxisome abundance during neuronal differentiation

Finally, we investigated the biological relevance of PKC-regulated peroxisome division. PKC activity varies between tissues, with the highest levels detected in the brain [101]. Further, peroxisome

bioRxiv preprint doi: https://doi.org/10.1101/2025.01.21.634043; this version posted January 25, 2025. The copyright holder for this preprint (which was not certified by peer review) is the author/funder, who has granted bioRxiv a license to display the preprint in perpetuity. It is made available under a CC-BY 4.0 International license.

regulation is critical for brain development, evidenced by the neurodegenerative conditions stemming from impaired peroxisome biogenesis [24]. We, therefore, tracked peroxisome abundance in differentiating neuronal cells. We used human neuroblastoma SH-SY5Y cells that can be differentiated into neuron-like cells that express neuronal markers after 18 days [102] (Figure 5A; Figure S7A and S7B). PKC activity was significantly increased in differentiating cells (Figure 5B), as was peroxisome number. We then differentiated SH-SY5Y neuronal cells in the presence of PKC inhibitor, that was added from day 10 to day 18 of neuronal differentiation. Apart from PAX6, differentiation markers, including MAP2, NeuN, and β-3 tubulin were upregulated to a similar extent in control and PKC-inhibited samples (Figure 5C; Figure S7B), but peroxisome number was decreased significantly (Figure 5D to F, Figure S7C). Similarly, we detected an increase in PKC activity and peroxisome number while differentiating iPSC to neuronal progenitor cells (Figure 5G-J; Figure S7D-F).

Discussion

We established a mechanistic connection between PKC activation and peroxisome biogenesis through PEX11b peroxisome formation. We showed that PKC promotes VAPB-dependent peroxisome biogenesis, through its established role in GSK3β inhibition and, a recently discovered, GSK3β regulation of peroxisome-ER interaction[68]. This mechanism allows cells to rapidly induce peroxisomes through signaling regulation, providing both an on-demand pool of functional peroxisomes and fulfilling the need for peroxisomal function during neuronal differentiation (Figure 5K).

PKC is a Serine/Threonine kinase that controls cell-to-cell recognition, cytoskeletal dynamics, GSK3 activity, membrane growth, eisosome assembly, T-cell development, apoptosis, response to oxidative stress, and lysosome biogenesis, among many other cellular functions [75, 76, 98, 103-114]. The PKC superfamily consists of 4 distinct sub-groups [75, 76] that share a kinase domain, and have a variety of regulatory domains that regulate spatiotemporal specificity [75] (Figure 2A). A screen of kinase inhibitor compounds revealed that inhibition of cPKC and nPKC results in a reduction of peroxisome numbers in human cell lines, including neuron-like cells. Peroxisome abundance is a balance between several pathways that produce and degrade peroxisomes, as well as PPARalpha-regulated transcriptional response that produces PEX peroxisome biogenesis factors [38, 46, 82]. Classical isoforms of PKC regulate PPAR alpha receptor [115]. One possibility is that PKC inhibition leads to reduced transcription of PEX genes, however we didn't see an effect of PKC inhibition on the PPAR transcriptional response. Another possibility is that PKC inhibition increases pexophagy. However, blocking pexophagy in normal conditions in human cells did not lead to a significant change in peroxisome number. The regulation of peroxisome abundance by pexophagy may be more relevant for clearance of peroxisomes, when excess peroxisomes are degraded, usually after a bout of upregulation [46, 81, 82, 89, 116]. The timing of PKC-induced peroxisome induction, as well as its dependence on PEX11b, suggested peroxisome division as the mechanism of PKC regulation. Our data showed that PKC positively regulates peroxisome-ER contact by modulating the ACBD5-VAPB tether by inhibiting GSK3β, which was recently shown to negatively regulate the contact[58, 68]. Although PKC can phosphorylate PEX11b on the N-terminus S53, the phosphorylation event is not sufficient to increase the number of peroxisomes. We also didn't observe any effect of PKC on PEX11b interaction with other division factors. It remains to be determined how peroxisome division depends on peroxisome-ER contact sites [117].

The PKC-regulated pathway that we have identified has broad implications for peroxisome physiology. For example, PKC and peroxisomes are known regulators of redox signaling, and peroxisomes both produce and clear hydrogen peroxide [118-120]. Both PKC and peroxisomes are known to control levels of D-serine in the brain [121-125]. The model of PKC-induced peroxisome proliferation also explains the notable increase in peroxisome abundance during neuronal differentiation. PKC activity has been recorded to be the highest in the brain, followed by liver and kidney [101], the organs which incidentally are primarily affected in peroxisome biogenesis disorders (Peroxisome Biogenesis Disorder/Zellweger syndrome, also known as cerebro-hepato-renal syndrome) [32, 126]. It would be of

bioRxiv preprint doi: https://doi.org/10.1101/2025.01.21.634043; this version posted January 25, 2025. The copyright holder for this preprint (which was not certified by peer review) is the author/funder, who has granted bioRxiv a license to display the preprint in perpetuity. It is made available under a CC-BY 4.0 International license.

interest to explore the peroxisomal contribution to diseases associated with abnormal PKC signaling, such as cancer, cardiovascular diseases, diabetes, psoriasis, and neurodegenerative disorders [127-133].

Acknowledgments

We thank Prof. Gisou van der Goot and Prof. Giovanni D'Angelo and members of their labs for their support, including access to essential equipment, reagents, and discussions. We thank Laurence Gouzi Abrami and Sylvia Ho for technical assistance. We thank the Gene Expression Core Facility (GECF, EPFL) for providing access to essential equipment and lenti-viral collection, Dr. Adrien Schmid and the Proteomics Core Facility (PCF) at EPFL for phospho-proteomic analysis, and the Bioimaging and Optics Core facility (PTBIOP, EPFL) for access to essential imaging equipment. We thank the Imaging and Microscopy centre (IMC) facility, University of Southampton. We thank Dr. Julien Schmidt and the Peptide and Tetramer Core Facility, University of Lausanne for peptide synthesis. We thank Prof. Ronald J. A. Wanders for the advice on radioactive measurements of peroxisomal fatty acid oxidation. We thank Prof. Doug Kellogg for a generous gift of the Pkc1 antibody. T.A. was funded by the HFSP Long-term Fellowship (LT000559/2021-L), EPFL Faculty, the University of Southampton, and the Wessex Medical Research Innovation Grant. A.B. was funded by the HFSPO Scientists for Scientists Initiative to help scientists affected by the war in Ukraine.

Author contributions: A. B., C. H., S. P. and T. A. performed the experiments. T. A. and D. K. designed the experiments, performed the data analysis, wrote the manuscript, and supervised the study.

Competing Interests: The authors declare that they have no competing interests.

Methods

Materials Availability

Reagents generated in this study are available upon request.

Data and Code Availability

Additional data that support the conclusions of this study are available upon request. This study didn't generate any code.

EXPERIMENTAL MODEL AND SUBJECT DETAILS

Human fibroblasts (AFF11), U2OS, HeLa, CHO, and HEK293T cells were maintained in high glucose DMEM supplemented with 10% fetal bovine serum (FBS), 1% penicillin/streptomycin, at 37°C/5% CO2, SH-SY5Y cells were maintained in high glucose DMEM/F12 1:1 media supplemented with 10% FBS, 1% penicillin/streptomycin at 37°C/5% CO2. Cells modified via CRISPR/Cas9 were maintained as above with addition of puromycin (1µg/ml, Sigma) or Blasticidin (5µg/ml, Sigma) during selection of the clonal populations. Neural progenitor cells were maintained in STEMdiff™ neural progenitor medium (STEM CELL Technologies). Neuronal differentiation of SH-SY5Y cells was done according to [102] with modifications, SH-SY5Y cells (initial seeding density 350,000 cells on 60mm dish) were gradually FBS starved for 10 days, before plating them on a Matrigel (Corning) extra-cellular matrix (seeding density (100,000 per a well of a 6-well plate), neuronal media was replaced every third day, cells were collected on day 18. Neuronal differentiation of induced pluripotent stem cells (iPSC) derived neuronal progenitor cells (NPC) [134] was done using STEMdiff™ neural differentiation kit (STEM CELL Technologies). The concentration of cells for plating was determined using cell counter (Countess II FL, Life Technologies) with the cell counting chambers (Invitrogen).

METHOD DETAILS

Antibodies

We used the following reagents to detect proteins: anti-GAPDH (sc-47724, Santa Cruz Biotechnology), anti-mCherry (34974, Invitrogen), anti-PMP70 (SAB4200181, Sigma), anti-PEX19

bioRxiv preprint doi: https://doi.org/10.1101/2025.01.21.634043; this version posted January 25, 2025. The copyright holder for this preprint (which was not certified by peer review) is the author/funder, who has granted bioRxiv a license to display the preprint in perpetuity. It is made available under a CC-BY 4.0 International license.

(14713-1-AP, Proteintech), anti-GFP (SAB4301138, Sigma), anti-NBR1 (16004-1-AP, Proteintech), anti-PEX11b (PA5-37011, Thermo Fisher Scientific), anti-PKC (P5704, Sigma), anti-Flag (F1804, Sigma), anti-myc (9E10, Sigma), anti-MFF (17090-1-aP, Proteintech), β-3 tubulin (D71G9, Cell Signaling Technology), anti-VAPB (14477-1-AP, ProteinTech).

Secondary antibodies for immunofluorescence: anti-Rabbit IgG Cy3-conjugated (Sigma-Aldrich C2306), anti-Mouse IgG Cy3-conjugated (Sigma-Aldrich C2181), anti-rabbit IgG Cy5 conjugated (Invitrogen A10523), Anti-Mouse IgG H&L (Alexa Fluor® 488) (Abcam).

Chemicals

Hoechst (Sigma), fatty acid free BSA (PAN), Phenylmethylsulfonyl fluoride (PMSF, Sigma), Go6983 (Cayman Chemicals), Behenic acid (VLCFA, Sigma), kinase screening library (Cayman Chemicals), D-Serine (Sigma), palmitic acid (LCFA, Sigma), Phorbol 12-myristate 13-acetate (Cayman Chemicals), siRNA NBR1 and control (Qiagen), oleic acid (Sigma), brain derived neurotrophic factor (BDNF, Stem Cell Technologies), Dibutyryl-cAMP (Santa Cruz Biotechnology), Neuropan 27 Supplement 50x (Pan Biotech).

CRISPR/Cas9

Knockout and endogenously tagged cell lines were constructed using CRISPR/Cas9 protocol and plasmids described in Ran et. al (Ran et al., 2013). Knockout cell lines were verified by western blotting, immunofluorescence. Genomic DNA was sequenced to verify disrupted region in knockout or the fidelity of endogenous tagging. Functional assay for knockout verification was performed where applicable (Reduced viability of PEX19 on VLCFA). Endogenous tagging was performed by fusing tagging construct (linker-GFP-polyA-Blasticidinn for C-terminal tagging of PMP70, and flag-GFP- for the N-terminal tagging of PEX11b) to the region upstream of the stop codon (~500bp) and downstream of stop codon (~500bp) for the C-terminal tagging, and to the region upstream of the start codon, and downstream of the start codon for the N-terminal tagging [135]. PCR product containing homologous regions flanking the tagging construct was co-transfected with px330-gRNA corresponding construct for C-terminal tagging and px459-gRNA construct for N-terminal tagging. Endogenous tagging was verified by western blotting, immunofluorescence staining, and genomic DNA sequencing. CRISPR specificity was profiled using Digenome-Seq web tool (http://www.rgenome.net/cas-offinder/) (Bae et al., 2014). Off targets were not found. The following target sequences are used to modify genomic DNA: endogenous tagging of PMP70 on the C-terminus – 5'-GTTGAGTTTGGCTCTTAGAGAAATC-3', endogenous tagging of PEX11b on the N-terminus – 5'-CGCGGAGCCTGGGCTGCGGCTGTCA-3', knockout of PEX19 – 5'-GGAGGTAGCAAGATGGCCGCCGCTG-3', knockout of PEX11b - 5'-CGCGGAGCCTGGGCTGCGGCTGTCA-3'.

Plasmid Construction:

All plasmids were constructed using *Escherichia coli* strain DH5α. Plasmids used in this study are summarized in the Table 1. We used px459 and px330 plasmids to clone CRISPR/Cas9 constructs for gene knockout and endogenous tagging. pSpCas9(BB)-2A-Puro (PX459) V2.0 was a gift from Feng Zhang (Addgene plasmid # 62988 ; http://n2t.net/addgene:62988 ; RRID:Addgene_62988) (Ran et al., 2013). pX330-U6-Chimeric_BB-CBh-hSpCas9 was a gift from Feng Zhang (Addgene plasmid # 42230 ; http://n2t.net/addgene:42230 ; RRID:Addgene_42230) (Cong et al., 2013). pcDNA4-PKCZeta WT His tagged was a gift from Jeff Wrana (Addgene plasmid # 24609 ; http://n2t.net/addgene:24609 ; RRID:Addgene_24609) [136]. PKC alpha WT was a gift from Bernard Weinstein (Addgene plasmid # 21232 ; http://n2t.net/addgene:21232 ; RRID:Addgene_21232) [137]. pWZL Neo Myr Flag PRKCD was a gift from William Hahn & Jean Zhao (Addgene plasmid # 20603 ; http://n2t.net/addgene:20603 ; RRID:Addgene_20603) [138]. HA GSK3 beta wt pcDNA3 was a gift from Jim Woodgett (Addgene plasmid # 14753 ; http://n2t.net/addgene:14753 ; RRID:Addgene_14753)[139]. pCDNA3.1-PPARA was a gift from Claes Wadelius (Addgene plasmid # 169019 ; http://n2t.net/addgene:169019 ; RRID:Addgene_169019)[140]. Human PEX3, PEX19, DAO, and ACBD5 were amplified from Lentiviral plasmid collection. Side Directed Mutagenesis was

bioRxiv preprint doi: https://doi.org/10.1101/2025.01.21.634043; this version posted January 25, 2025. The copyright holder for this preprint (which was not certified by peer review) is the author/funder, who has granted bioRxiv a license to display the preprint in perpetuity. It is made available under a CC-BY 4.0 International license.

verified by sequencing. Site directed mutagenesis was performed to obtain PEX11b mutants, and GSK3bS9A.

Table 1. Plasmids used in this study

Plasmid name	Source
pcDNA3.1 mCH*4skl	[134]
pcDNA3.1 GSK3beta	Addgene 14753
pcDNA3.1 PPARA	Addgene 169019
pcDNA3.1 PEX3hismyc	This study
pcDNA3.1 flagPEX19	This study
Px459-PEX19 KO	[66]
Px330-PMP70-C	This study
Px459-PEX11b-N	This study
pCtag-PMP70-GFP-Blasti	This study
pNtag-PEX11b-flag-GFP	This study
pcDNA3.1- PKCα-mCherry	This study, PKCα is from Addgene 21232
pcDNA3.1 PKCδ -mCherry	This study, PKCδ is from Addgene 20603
pcDNA3.1- PKCζ -mCherry	This study, PKCζ is from Addgene 24609
pcDNA3.1 hismyc-PEX11b	This study
pcDNA3.1 hismyc-PEX11b S53D	This study
pcDNA3.1 hismyc-PEX11b S53A	This study
pEGFP-VAPB	[141]
pcDNA3.1 hismyc-ACBD5	This study
pcDNA3.1 GFP-SKL	This study
pcDNA3.1 ER-mCherry	[134]

PKC activity

Protein kinase activity was determined by PKC Kinase Activity Assay Kit (Abcam) according to the manufacturer instructions. Protein concentration in lysates was quantified using bicinchoninic acid (BCA) Assay kit (Interchim).

Peroxisome abundance measurement

We used peroxisome density as a read-out for peroxisome abundance in this study. To calculate the number of peroxisomes cells were visualized by confocal microscopy. Images were captured using the same parameters between conditions within the experiment. Images were analyzed by Fiji (ImageJ) software, peroxisome numbers were quantified as maxima of intensity in the cytoplasmic space and the number was divided by the size of the areas (square micron) which results in a peroxisome per square micron cytoplasmic ratio. The cytoplasmic space was defined using threshold mask that excludes the nuclei (stained with Hoechst) and background using ImageJ Threshold function. The resultant area was divided into N parts equal to the number of cells (nuclei number). At least 100 areas were quantified per condition per experiment. 2D areas with a nucleus in focus were chosen for all of the experiments, because 3D projections often create overlaps between peroxisomal compartments.

Preparing samples for the Mass spectroscopy

Cells expressing CRISPR/Cas9 flag-GFP-PEX11b were grown to 80% confluency in the presence of VLCFA for 2 days, washed with PBS, and lysed in 1%TritonX-100 50mM Tris HCl pH7.4, 150mM NaCl buffer at 4°C for 30min. PEX11b was purified using Anti-FLAG M2 affinity gel (Sigma). 10% of the sample was collected for the Western Blot analysis. Beads were collected and washed free of detergents in 50mM Tris HCl, pH7.4 150mM NaCl. Samples were reduced in 10 mM dithioerythritol (DTE) alkylated in 55 mM iodoacetamide (IAA)). Digestion was performed overnight at 37 °C using

bioRxiv preprint doi: https://doi.org/10.1101/2025.01.21.634043; this version posted January 25, 2025. The copyright holder for this preprint (which was not certified by peer review) is the author/funder, who has granted bioRxiv a license to display the preprint in perpetuity. It is made available under a CC-BY 4.0 International license.

mass spectrometry grade trypsin and LysC protease (Thermo Fisher Scientific). The following day, protein digests were then subjected to C18 stage tip cleaning, dried in a speed-vacuum and stored at -20°C until LC-MS analysis.

LC/MS/MS analysis (shotgun approach)

Mass spectrometry-based proteomics-related experiments were performed by the Proteomics Core Facility at EPFL. Mass spectrometry (MS) analysis was performed on an Orbitrap Exploris 480 mass spectrometer (Thermo Fisher Scientific) coupled to a nano-UPLC Dionex pump. For liquid chromatography (LC) MS/MS analysis, trypsin / LysC digested samples were resuspended in 30-60ul of a mobile phase A solution (2% ACN / water, 0.1% formic acic) and then separated by reversed-phase chromatography using a Dionex Ultimate 3000 RSLC nanoUPLC system on a home-made 75 µm ID × 50 cm C18 capillary column (Reprosil-Pur AQ 120 Å, 1.9 µm) in-line connected with the MS instrument. Peptides were separated by applying a non-linear 90min gradient ranging from 99% solvent A (2% ACN and 0.1% FA) to 90% solvent B (90% ACN and 0.1%FA) at a flow rate of 250nl/min. For spectral library and charge state determination of Pex11b peptides, the MS instrument was operated in data-dependent mode (DDA). Full-scan MS spectra (300−1500 m/z) were acquired at a resolution of 120’000 at 200 m/z. Data-dependent MS/MS spectra were recorded followed by HCD (higher-energy collision dissociation) fragmentation on the ten most intense signals per cycle (2 s), using an isolation window of 1.4 m/z. HCD spectra were acquired at a resolution of 60’000 using a normalized collision energy of 32 and a maximum injection time of 100 ms. The automatic gain control (AGC) was set to 100’000 ions. Charge state screening was enabled such that unassigned and charge states higher than six were rejected. Precurors intensity threshold was set at 5’000. Precursor masses previously selected for MS/MS acquisition were excluded from further selection for a duration of 20 s, and the mass exclusion window was set at 10 ppm.

MS data processing and database searches

PEAKS Studio X+ Pro (Bioinformatics Solutions Inc.) software was used for data processing. The raw MS data files were imported into PEAKS Studio software using the following parameters for the database search: For protein identification, the UniProt/Swiss-Prot human proteome data base (UP000005640) or searched using the canonical protein sequence of human Pex11b (accession#: O96011) combined with a decoy and contaminant database was used. For peptide identification the following settings were used: Enzyme: Trypsin, missed cleavages: 2 precursor mass tolerance: 10 ppm, fragment mass tolerance: 0.1 Da, minimum charge: 2, maximum charge: 5, fixed modifications: Carbamidomethyl (C), variable modifications: Oxidation (M), phosphorylation (STY). False discovery rate (FDR) was calculated based on the target/decoy database and peptides as well as proteins with FDR threshold of $\leq 1\%$ (or -log10P $\geq$15 for peptides) were chosen as true positive hits. The PTM identification threshold (PEAKS) was set at the recommended AScore of -log10P of 20 (p=0.01).

RNA preparation and real time PCR (rtPCR)

Total mRNA was extracted from cells using RNeasy Mini Kit (Qiagen). cDNA synthesis was performed using iScript cDNA synthesis kit (Biorad). Real time PCR was performed using QuantStudio6 (Thermo Fischer Scientific). mRNA levels were quantified using QuantStudio6 software. Experiments were repeated three times with 2 technical repeats and fold difference in expression was calculated by ΔΔCt method using GAPDH as a housekeeping gene (Livak and Schmittgen, 2001).

Table 2: Primers for rtPCR

NT5F	5’-GTGGGAATCGTTGGATACACTTCC
NT5R	5’-CAAAACCCGAATGTCCCAGTGC

bioRxiv preprint doi: https://doi.org/10.1101/2025.01.21.634043; this version posted January 25, 2025. The copyright holder for this preprint (which was not certified by peer review) is the author/funder, who has granted bioRxiv a license to display the preprint in perpetuity. It is made available under a CC-BY 4.0 International license.

NESF	5'-GGGCCTACAGAGCCAGATCG
NESR	5'-CTGAAAGCTGAGGGAAGTCTTGG
NeuNF	5'-CACACCAGCACAGACCCACC
NeuNR	5'-GATGTTGGAGACGTGTAGCCGC
MAP2F	5'-GGGAGGATGAAGAGGGTGCC
MAP2R	5'-CAGGACTGCTACAGCCTCAGC
PAX6F	5'-GGAATCAGAGAAGACAGGCCAGC
PAX6R	5'-CCATGGTGAAGCTGGGCATAG
GAPDHF	5'-GGGGAAGGTGAAGGTCGGAGTC
GAPDHR	5'-GTGCCATGGAATTTGCCATGGG
PEX5F	5'-CCTGCAGGACCAGAATGCAC
PEX5R	5'-CTGAGTTACATCCACAGCATCTCC
PEX19F	5'-CAGCACCCCCTTCTACCACC
PEX19R	5'-GGAACTGCTCCACCAGGTG
PEX7F	5'-ACAACGAACATGTCCTCATCACC
PEX7R	5'-GAGCCAGACACCACAAGCTG
CATF	5'-GCATGCTAAAGGAGCAGGGG
CATR	5'-GTCAGCTGAACCCGATTCTCC
BAATF	5'-CCTCCTTGGCCTTGGCTTACC
BAATR	5'-CTCCTTGACATACAGAGACTACCCC
ACOX2F	5'-GTGGACATGGCAAGAACAGCC
ACOX2R	5'-ACTGGAACAGGCGTTCGTAGAC
DBPF	5'-CAAAGTTGGGTCTTCTGGGCC
DBPR	5'-GCCACATACTCTGGCTTCAGGG
SCPxF	5'-GTATGGCCTGCAATCCAAAGC
SCPxR	5'-GTGTCAGGCCAGATTTCTCATAGCA
AMACRF	5'-TTTGCTGGTGGTGGCCTTATG
AMACRR	5'-TCGAGGTGCTTCCCACAGAC
ACAA1F	5'-GAATCTGAGGCCGGAACAGC
ACAA1R	5'-ACCTGCTATGCTGGCCACTG
ACOX1F	5'-GTCAGGTCCTTCCTTGTGGGAG
ACOX1R	5'-GTATGCGCCCACAAACTGGAAG
PHYHF	5'-CGAAGGTCCAGGATTTCCAGG
PHYHR	5'-TAGTGCAGGTCCTGGTGCAG
DAOF	5'-CTGACCCCAACAACCCACAG
DAOR	5'-CCGAAATCCCAGAACTGTGTCC
PEX3F	5'-CAGAAATCTCGTTGAGCAGCATAAGTC
PEX3R	5'-CTAAAATCTGGGCTTTCCAACATGTCTC

Co-Immunoprecipitation

Harvested cells were lysed with CHAPS (1%) in 50mM Tris-HCl pH7.4, 150mM NaCl with a complete protease inhibitor cocktail (Pierce) for 20 min at 4°C with rotation (1%CHAPS in PBS for ACBD5 immunoprecipitation). After 1 min 10,000g centrifugation the supernatant was incubated with protein G Sepharose (GE Healthcare) for 30min at 4°C with rotation. After 1min 10,000g centrifugation 10% of the supernatant was collected as an Input, and the resulting supernatant was

bioRxiv preprint doi: https://doi.org/10.1101/2025.01.21.634043; this version posted January 25, 2025. The copyright holder for this preprint (which was not certified by peer review) is the author/funder, who has granted bioRxiv a license to display the preprint in perpetuity. It is made available under a CC-BY 4.0 International license.

incubated with 25µl of Myc-Trap Agarose beads (Chromotek) overnight at 4°C with rotation. After the incubation the beads were washed 4 times for 5 min with the lysis buffer at 4°C with rotation. Before loading on the gel, the beads and input were boiled with a sample buffer. Equal amounts of Input and Eluted bead sample were loaded on the SDS-PAGE.

Immunofluorescence

Cells were grown on glass bottom plates or glass slides, fixed using 4% paraformaldehyde in phosphate buffered saline (PBS) for 10 minutes, washed with PBS, permeabilized with 0.5% Triton X100, then blocked overnight in 5% BSA in PBS prior to antibody staining.

Radioactive measurement of beta fatty acid oxidation using 13,14-3H docosanoic acid (C22:0)

Cells were grown in 12-well plates with initial plating density of 100 000 cells per well for two days. Cold C22:0 (4 µM) and 13,14-3H C22:0 (1 µCi, Anawa) were mixed with the media and added to the cells for 20 hours. Media was collected and processed according to [142, 143] with minor modifications. Radioactivity was quantified in the media and water fractions transferred to the Scintillation vials after 3 days using scintillation counter. Cold samples, and cell-free samples were used as controls and background subtraction. Peroxisome deficient cells were used as a control to distinguish between peroxisomal and mitochondrial fatty acid oxidation.

Microscopy

For live cell imaging 4-well microscope glass bottom plates (IBIDI) or Cellview cell culture dish (Greiner Bio One) were used. Alternatively, cells were grown on glass slides (Marienfeld). Confocal images and movies were acquired using SP8 (Leica) confocal microscope equipped with a temperature and CO2 incubator, using a 60x PlanApo VC oil objective NA 1.40. We used 406nm, 488nm, 561nm, and 640nm lasers. Peroxisome tracking in the movies was done using TrackMate Fiji plugin[144]. Super resolution microscopy was done using STED microscope (Leica TCS SP8 STED 3X) with a 100 × 1.4 NA oil-immersion objective. Image processing was performed using Fiji (ImageJ) software.

Peptide phosphorylation competition assay

Peptides were synthesized by the Peptide and Tetramer core Facility, University of Lausanne. The following peptides were used for the assay: PEX11b-1 GCGGLESHLSLGRKL, PEX11b-2 GCGGADALESAKRAV, PEX11b-3 GCGGKWAQRSFRYYL, PEX11b-4 GCGGRYYLFSLIMNL, PEX11b-5 GCGGESSACSRRLKG;PEX11b-6 GCGGRRLKGSGGGVP, PKCa-Control GCGGFKKQGSFAKKK [95]. 100ng of pure peptides were mixed with or without 100ng of pure PKC, and incubated according to the PKC activity assay kit (Abcam). Peptides were then subjected to mass spectrometry.

QUANTIFICATION AND STATISTICAL ANALYSIS

Three or more independent experiments were performed to obtain the data. P values were calculated by two-tailed Student t-test, or one-way ANOVA for samples following normal distribution determined by the Shapiro-Wilks test. The equality of variances was verified by Brown-Forsythe or F test. Mann-Whitney (2 groups), or Kruskal-Wallis (multiple groups) tests were used for samples that didn't follow a normal distribution. The sample sizes were not predetermined. Refer to the Supplementary Table 3 for the details on statistical analysis.

Supplemental Items

Table S1. Kinase Inhibitor Screen
Table S2. Phosphorylation of PEX11b in VLCFA conditions
Table S3. Statistical Analysis
Supplementary Movies 1-6
Supplementary Figures S1-S10

bioRxiv preprint doi: https://doi.org/10.1101/2025.01.21.634043; this version posted January 25, 2025. The copyright holder for this preprint (which was not certified by peer review) is the author/funder, who has granted bioRxiv a license to display the preprint in perpetuity. It is made available under a CC-BY 4.0 International license.

Fig. 1. Kinase Inhibitor screen reveals signaling regulators of peroxisome abundance

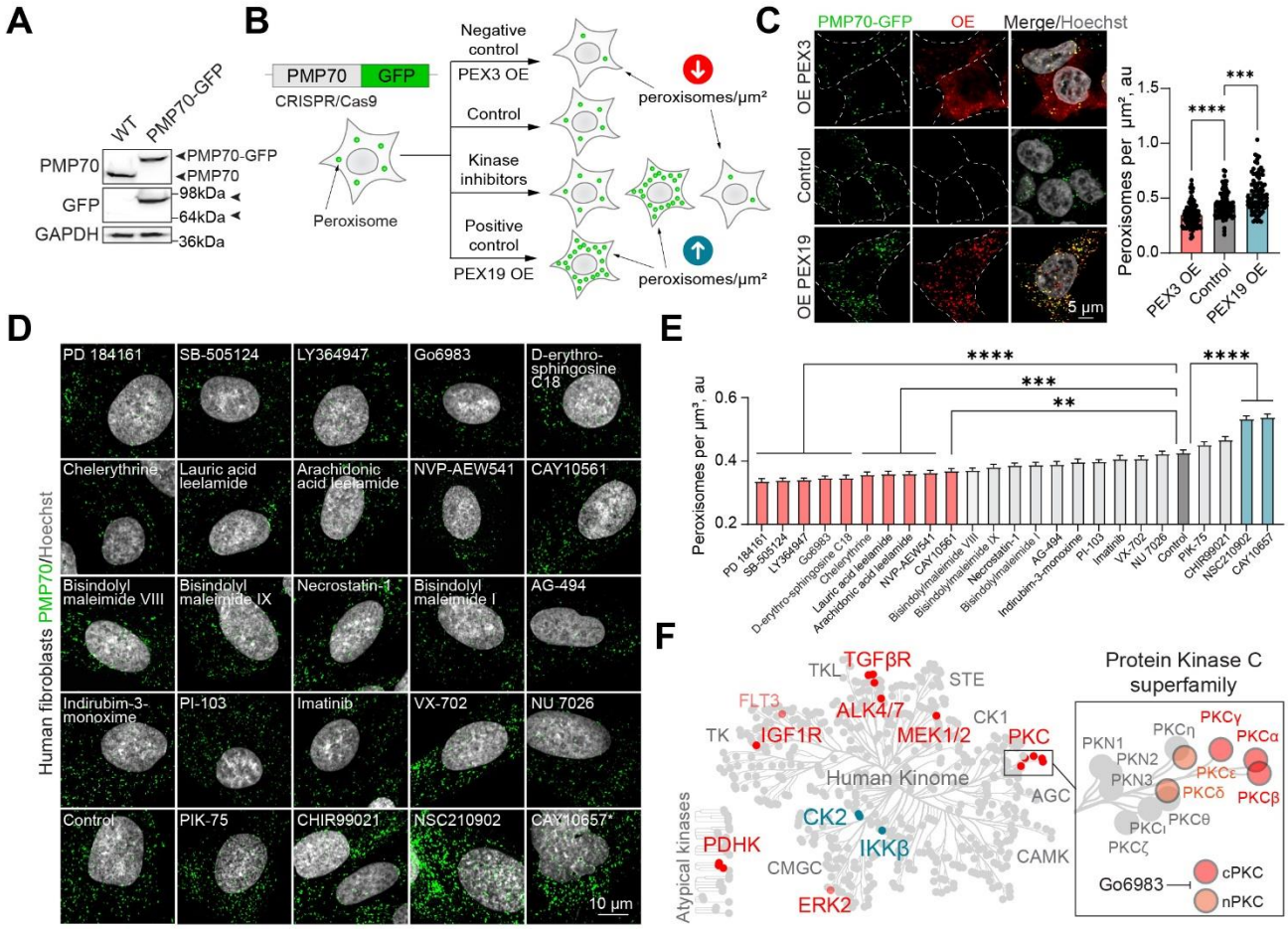

Figure 1 Kinase Inhibitor screen reveals signaling regulators of peroxisome abundance

(A) Western blot of WT and CRISPR/Cas9 PMP70-GFP HEK293T cells. Arrow heads indicate the size shift of the tagged PMP70-GFP.

(B) Schematic of the peroxisome biogenesis regulators screen. CRISPR/Cas9 PMP70-GFP HEK293T cells were incubated in control or 1µM of small molecules for 2 days, PEX3 overexpression was used as a negative control, and PEX19 overexpression was used as a positive control. Refer to Figure S1F to G, S2, and S3 for the screen details.

(C) Confocal microscopy of CRISPR/Cas9 PMP70-GFP HEK293T cells overexpressing PEX3-myc, flag-PEX19, or an empty vector. Quantification shows the number of peroxisomes per square micron of the cytoplasm in the 2D confocal image, mean± SEM, N=100, *** - p<0.001, **** - p<0.0001.

(D-E) Confocal microscopy of peroxisomes in human primary fibroblasts AFF11 treated with indicated kinase inhibitors for 2 days. Peroxisomes were visualized using PMP70 antibody, nuclei were stained with Hoechst (10µg/ml). Representative images are shown, Scale bar - 10µm, * - abnormal nuclear morphology. (E) Quantification shows the number of peroxisomes per square micron of the cytoplasm in the flattened 3D image (indicated as cubic micron), mean± SEM, N=100, ** - p<0.01, *** - p<0.001, **** - p<0.0001.

(F) Identified kinase inhibitors plotted on the human kinome network [145, 146]. Positive regulators (inhibition decreases number of peroxisomes) are indicated in red, negative regulators (inhibition

bioRxiv preprint doi: https://doi.org/10.1101/2025.01.21.634043; this version posted January 25, 2025. The copyright holder for this preprint (which was not certified by peer review) is the author/funder, who has granted bioRxiv a license to display the preprint in perpetuity. It is made available under a CC-BY 4.0 International license.

increases the number of peroxisomes) are indicated in blue. Protein Kinase C superfamily is shown in the inlet, cPKC – classical PKC, nPKC – novel PKC isoforms, G06983 inhibits indicated PKC isoforms.

Fig. 2. Protein Kinase C Delta positively regulates peroxisome abundance

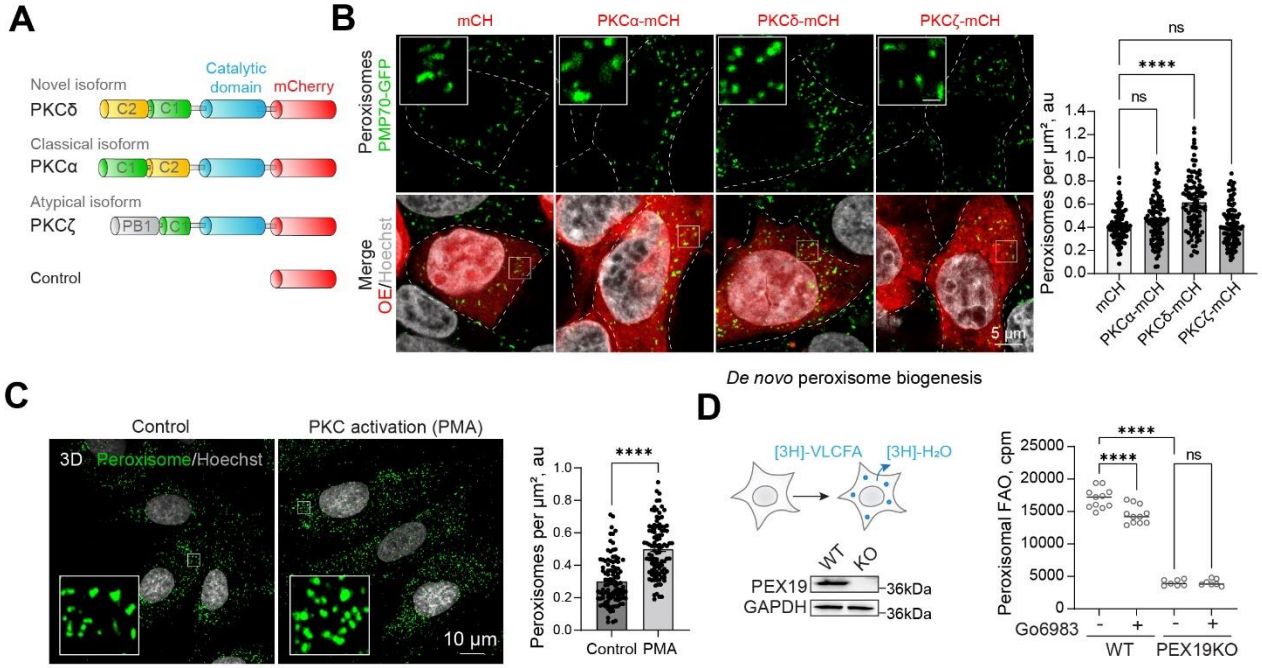

Figure 2 Protein Kinase C Delta positively regulates peroxisome abundance

(A) Schematic of different PKC isoforms used in (B)

(B) Confocal microscopy of HEK293T CRISPR/Cas9 PMP70-GFP cells overexpressing (OE) PKCα-mCherry, PKCδ-mCherry, or PKCζ-mCherry. Quantification shows number of peroxisomes per square micron of the cytoplasm in the 2D confocal image, mean± SEM, N=100, **** - p<0.0001. Scale bar - 5μm Refer to Figure S5H.

(C) Confocal microscopy of peroxisomes in human primary fibroblasts AFF11 treated with PMA (0.5μM) for 1 day. Peroxisomes were visualized using PMP70 antibody, nuclei were stained with Hoechst (10μg/ml). Representative images are shown, Scale bar - 10μm. Quantification shows number of peroxisomes per square micron, mean± SEM, N=103, **** - p<0.0001. Refer to Figure S5I.

(D) Radioactive peroxisomal FAO measurement using 3H-docosanoic acid in HEK293T WT or PEX19KO in control or Go6983 (5μM for 48hours) conditions. Quantification shows the number of counts per minute, mean± SEM, N=6-12, *** - p<0.001, ****

bioRxiv preprint doi: https://doi.org/10.1101/2025.01.21.634043; this version posted January 25, 2025. The copyright holder for this preprint (which was not certified by peer review) is the author/funder, who has granted bioRxiv a license to display the preprint in perpetuity. It is made available under a CC-BY 4.0 International license.

Fig. 3. Protein kinase C regulation depends on PEX11b

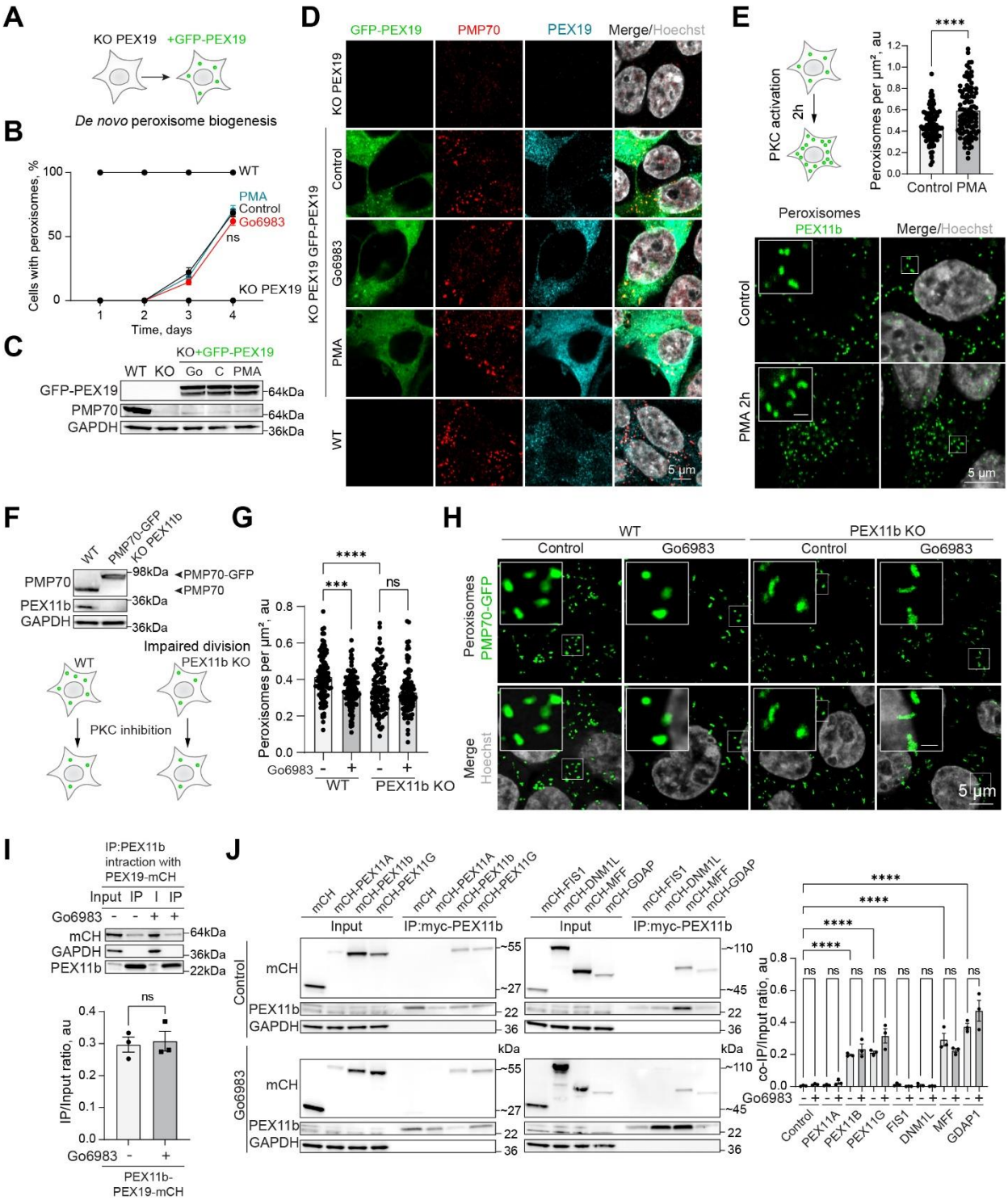

Figure 3 Protein kinase C regulation depends on PEX11b

(A) Schematic of PEX19 complementation assay.

(B-D) Confocal microscopy of the peroxisomes in HEK293T WT, PEX19 KO, and PEX19 KO cells overexpressing flag-GFP-PEX19 in control, Go6983 1µM, and PMA 0.5µM conditions. Cells were

bioRxiv preprint doi: https://doi.org/10.1101/2025.01.21.634043; this version posted January 25, 2025. The copyright holder for this preprint (which was not certified by peer review) is the author/funder, who has granted bioRxiv a license to display the preprint in perpetuity. It is made available under a CC-BY 4.0 International license.

fixed and visualized on identified days. (B) Quantification shows the ratio of cells that restored peroxisomes among the transfected cells. Scale bar - 5µm. (C) Western blot of PMP70 expression on day 4 of the complementation assay.

(E) Confocal microscopy of peroxisomes in HEK293T CRISPR/Cas9 flag-GFP-PEX11b cells treated with 0.5µM PMA for 2 hours. Nuclei were stained with Hoechst (10µg/ml). Representative images are shown, Scale bar - 5µm, inlet - 1µm. Quantification shows number of peroxisomes per square micron of the cytoplasm in the 2D confocal image, mean± SEM, N=100, **** - p<0.0001.

(F) Western blot of PEX11b and PMP70 in the WT and CRISPR/Cas9 PMP70-GFP PEX11b KO HEK293T cells. Arrow heads indicate the size shift of the tagged PMP70-GFP.

(G-H) Confocal microscopy of peroxisomes in HEK293T CRISPR/Cas9 PMP70-GFP WT and PEX11b KO cells grown in control or Go6983 5µM conditions. Nuclei were stained with Hoechst (10µg/ml). Representative images are shown, Scale bar - 5µm, inlet - 1 µm. Quantification shows the number of peroxisomes per square micron of the cytoplasm in the 2D confocal image, mean± SEM, N=100, *** - p<0.001, **** - p<0.0001.

(I) Co-Immunoprecipitation of mycPEX11b in control and PKC inhibition conditions (Go6983 5µM, 24 hours). Western blot of mycPEX11b and mCherry-PEX19 in the WT HEK293T cells. Quantification shows the IP to Input (I) ratio, mean± SEM, N=3.

(J) Co-Immunoprecipitation of mycPEX11b and peroxisome division factors in control and PKC inhibition conditions (Go6983 5µM, 24 hours). Western blot of mycPEX11b and mCherry-, mCherry-PEX11A, PEX11b, PEX11G, FIS1, DNM1L, MFF, or GDAP1 in the WT HEK293T cells. Quantification shows the IP to Input (I) ratio, mean± SEM, N=3, **** - p<0.0001.

bioRxiv preprint doi: https://doi.org/10.1101/2025.01.21.634043; this version posted January 25, 2025. The copyright holder for this preprint (which was not certified by peer review) is the author/funder, who has granted bioRxiv a license to display the preprint in perpetuity. It is made available under a CC-BY 4.0 International license.

Fig. 4. PKC regulates peroxisome-ER VAP-dependent interaction through GSK3β inhibition

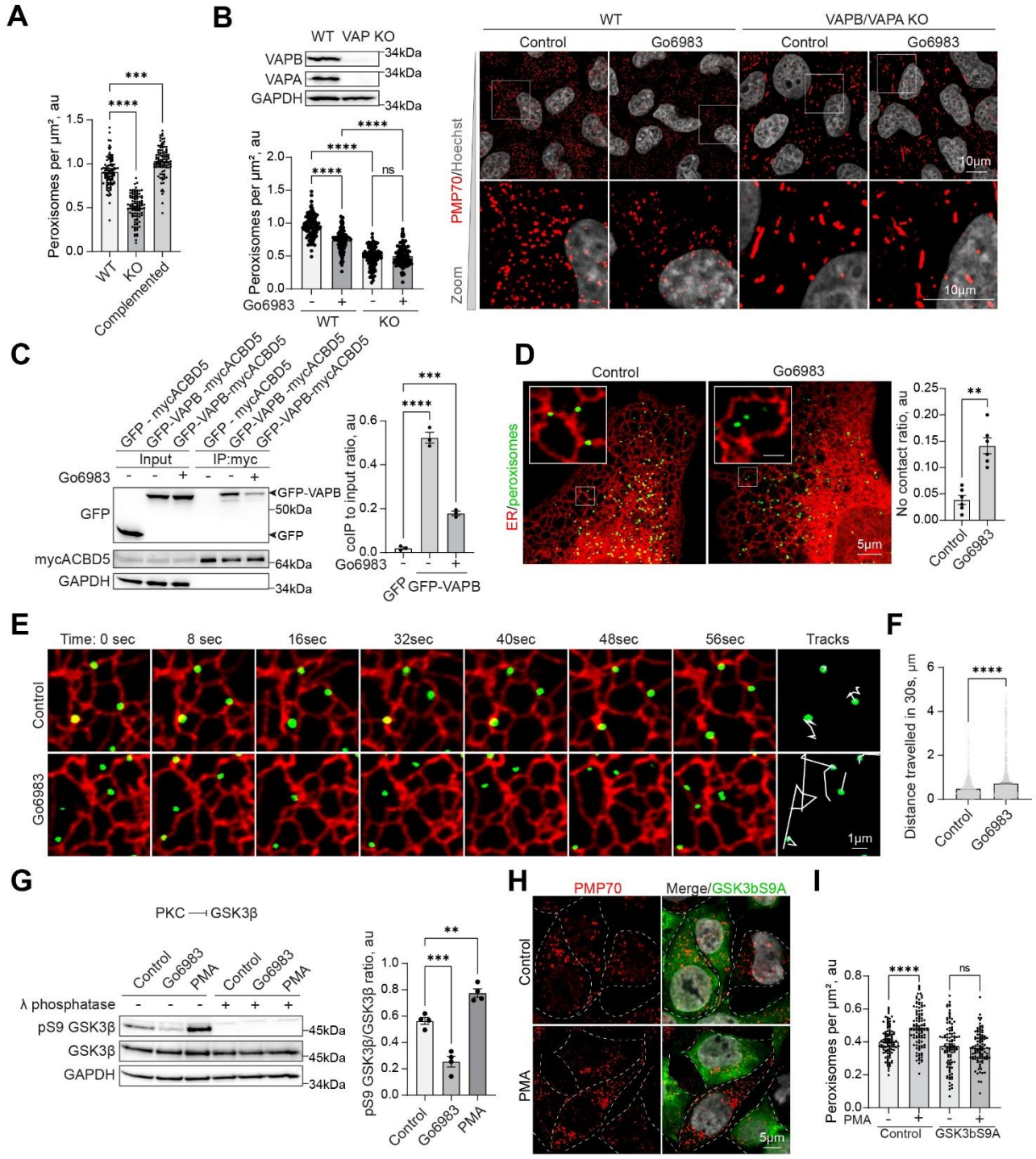

Figure 4 PKC regulates peroxisome-ER VAP-dependent interaction through GSK3b inhibition

(A) Quantification of confocal microscopy of peroxisomes stained with antiPMP70 antibody in WT and VAPB/VAPA KO HeLa cells in control and GFP-VAPB overexpression conditions. Quantification shows the number of peroxisomes per micron square, mean± SEM, N=100, *** - p<0.001, **** - p<0.0001. Refer to figure S4H

bioRxiv preprint doi: https://doi.org/10.1101/2025.01.21.634043; this version posted January 25, 2025. The copyright holder for this preprint (which was not certified by peer review) is the author/funder, who has granted bioRxiv a license to display the preprint in perpetuity. It is made available under a CC-BY 4.0 International license.

(B) Confocal microscopy of peroxisomes stained with anti-PMP70 antibody in WT and VAPB/VAPA KO HeLa cells in control Go6983 (5μM for 48hours). Quantification shows the number of peroxisomes per micron square, mean± SEM, N=100, *** - p<0.001, **** - p<0.0001. Western blot confirming the KO is shown.

(C) Co-Immunoprecipitation of mycACBD5 in control and PKC inhibition conditions (Go6983 5μM, 24 hours), mycACBD5 and GFP or GFP-VAPB were overexpressed in HEK293T cells. Quantification shows the IP to Input ratio, mean± SEM, N=3, *** - p<0.001, **** - p<0.0001.

(D-F) Live cell confocal microscopy of ER and peroxisomes in U2OS cells in control and Go6983 conditions. Quantification shows the ratio of peroxisomes that are not proximal or overlapping with the ER, mean± SEM, N=6 pooled from 1000 peroxisomes in at least 30 cells per condition, ** - p<0.01, and a distance travelled by a single peroxisome in 30seconds, mean± SEM , N=1000, **** - p<0.0001.

(G) Western blot of GSK3β inhibitory S9 phosphorylation in PMA(0.5μM for 2hours) and Go6983 (5μM for 4hours) conditions. Quantification shows the ratio of phosphorylated pS9 GSK3β to non-phosphorylated GSK3β, mean± SEM, N=4, *** - p<0.001, ** - p<0.01.

(H) Confocal microscopy of peroxisomes stained with antiPMP70 antibody in HEK293T control or overexpression of GSK3β S9A mutant in control or PMA (0.5μM for 4hours) conditions. (I) Quantification shows the number of peroxisomes per micron square, mean± SEM, N=100, **** - p<0.0001.

bioRxiv preprint doi: https://doi.org/10.1101/2025.01.21.634043; this version posted January 25, 2025. The copyright holder for this preprint (which was not certified by peer review) is the author/funder, who has granted bioRxiv a license to display the preprint in perpetuity. It is made available under a CC-BY 4.0 International license.

Fig. 5. Protein kinase C regulates peroxisome abundance in neuronal differentiation

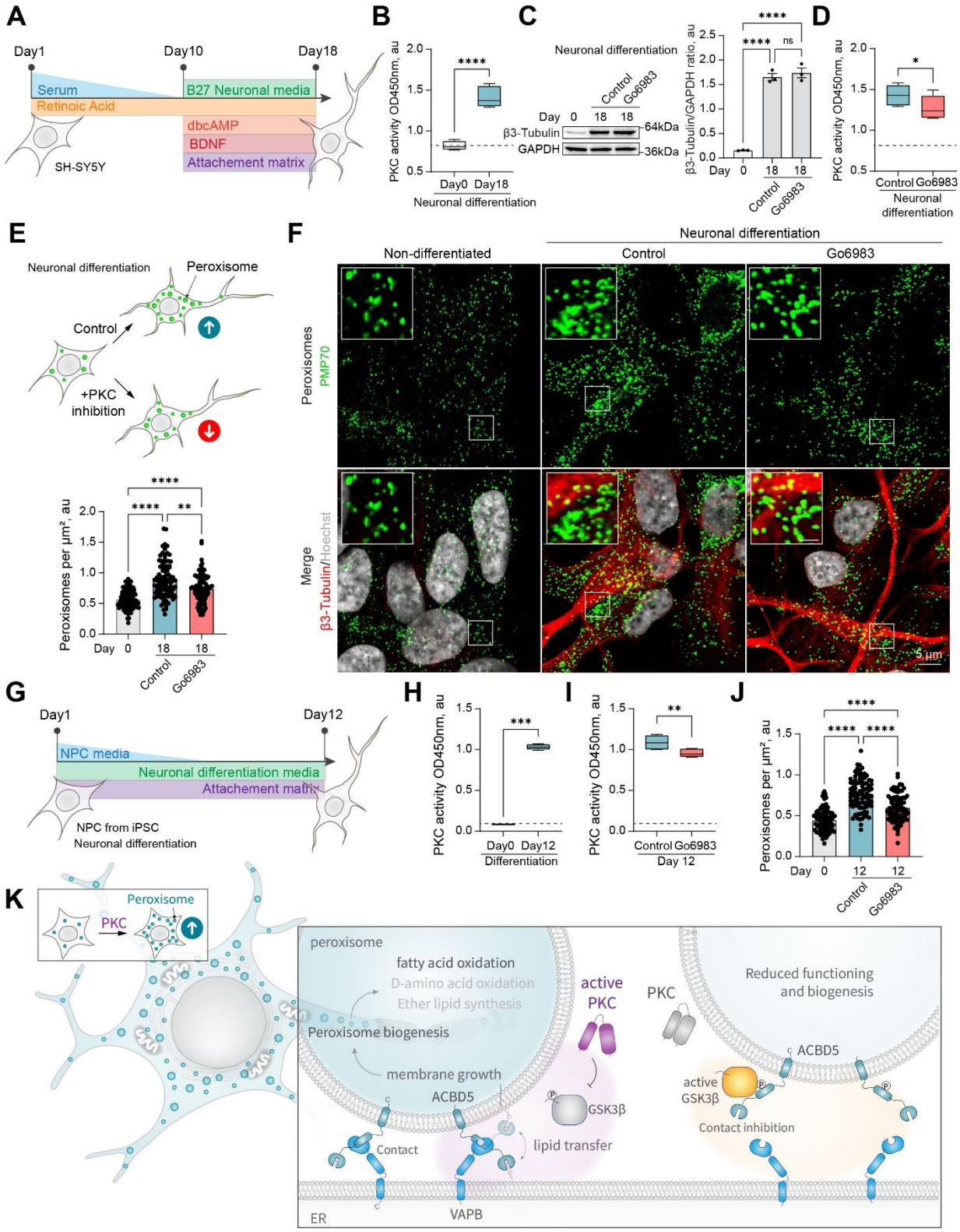

Figure 5 Protein kinase C regulates peroxisome abundance in neurons

(A) Schematic of the SH-SY5Y neuronal differentiation.

bioRxiv preprint doi: https://doi.org/10.1101/2025.01.21.634043; this version posted January 25, 2025. The copyright holder for this preprint (which was not certified by peer review) is the author/funder, who has granted bioRxiv a license to display the preprint in perpetuity. It is made available under a CC-BY 4.0 International license.

(B) PKC activity in the non-differentiated and 18-day differentiated SH-SY5Y cells. Quantification shows PKC activity, mean± SEM, N=10, **** - p<0.0001.

(C) Western blot of β-3 tubulin in the non-differentiated and 18-day differentiated SH-SY5Y cells in control and Go6983 1μM conditions, Go6983 was added on days 10-18 of the differentiation protocol. Quantification shows the ratio of and β-3 tubulin to GAPDH, mean± SEM, N=3, **** - p<0.0001.

(D) PKC activity in the 18-day differentiated SH-SY5Y cells in control and Go6983 1μM conditions, Go6983 was added on days 10-18 of the differentiation protocol. Quantification shows PKC activity, mean± SEM, N=10, * - p<0.05.

(E-F) Confocal microscopy of peroxisomes in the non-differentiated and 18-day differentiated SH-SY5Y cells in control and Go6983 1μM conditions, Go6983 was added on days 10-18 of the differentiation protocol. Peroxisomes were visualized with the PMP70 antibody, nuclei were stained with Hoechst (10μg/ml), and neuronal differentiation was visualized with β-3 tubulin antibody. Representative images are shown, Scale bar - 5μm, inlet - 1μm. (F) Quantification shows the number of peroxisomes per square micron of the cytoplasm in the 2D confocal image, mean± SEM, N=102, **** - p<0.0001. Refer to Figure S12C.

(G) Schematic of the neuronal progenitor cells (NPCs) neuronal differentiation.

(H) PKC activity in the non-differentiated and 12-day differentiated NPCs. Quantification shows PKC activity, mean± SEM, N=8, **** - p<0.0001.

(I) PKC activity in the 12-day differentiated NPCs in control and Go6983 1μM conditions, Go6983 was added on days 1-12 of the differentiation protocol. Quantification shows PKC activity, mean± SEM, N=8, ** - p<0.01.

(J) Quantification of the number of peroxisomes per square micron of the cytoplasm in the 2D confocal image in the non-differentiated and 12-day differentiated NPCs in control and Go6983 1μM conditions, Go6983 was added on days 1-12 of the differentiation protocol, mean± SEM, N=90, **** - p<0.0001. Refer to Figure S12E.

(K) Model of PKC regulation of peroxisome abundance

bioRxiv preprint doi: https://doi.org/10.1101/2025.01.21.634043; this version posted January 25, 2025. The copyright holder for this preprint (which was not certified by peer review) is the author/funder, who has granted bioRxiv a license to display the preprint in perpetuity. It is made available under a CC-BY 4.0 International license.

Supplementary Figure S1

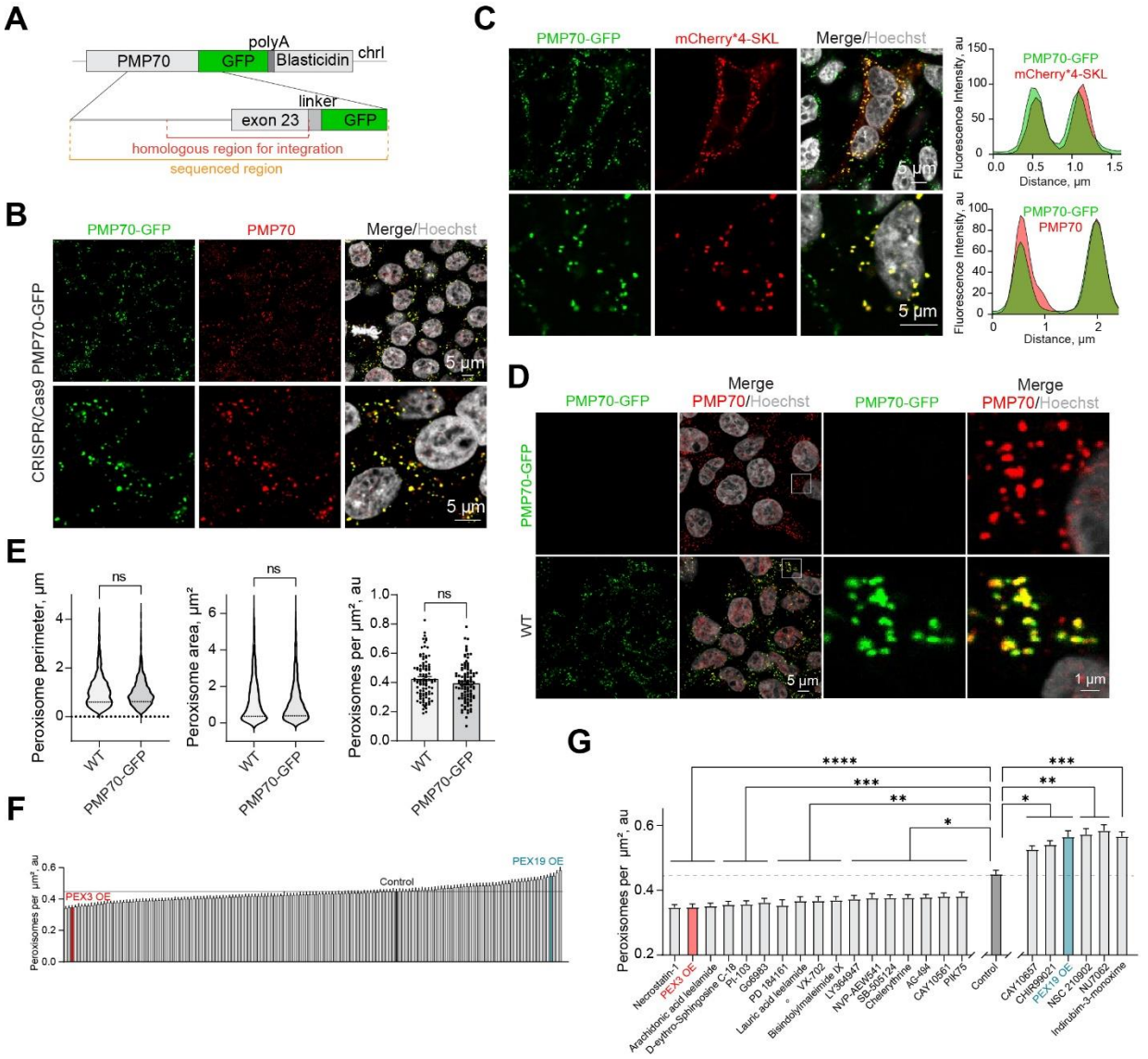

Figure S1.

(A) Schematic of the genomic DNA region corresponding to the end of the human PMP70 open reading frame endogenously tagged with -GFP-polyA-Blasticidin.

(B-C) Confocal microscopy of the peroxisomal import marker mCherry*4-SKL expressed in HEK293T PMP70-GFP, and (**B**) a confirmation of the PMP70-GFP peroxisomal localization. The fluorescence intensity profiles through single peroxisomes are shown. Scale bar - 5µm.

(D-E) Comparison of WT and PMP70-GFP tagged HEK293T. Confocal images and quantification of perimeter (N=1000), area (N=1000), and density of peroxisomes (N=100) are shown, mean± SEM.

(F-G) Quantification of the number of peroxisomes per square micron of the cytoplasm in the HEK293T cells treated with 1µM of the indicated small molecule, mean± SEM, * - p<0.05, ** - p<0.01, *** - p<0.001, **** - p<0.0001. **(D)** – significant screen hits are plotted, **(E)** complete screen. Refer to Figure S2 and S3 for the confocal images, N=100 for each molecule.

bioRxiv preprint doi: https://doi.org/10.1101/2025.01.21.634043; this version posted January 25, 2025. The copyright holder for this preprint (which was not certified by peer review) is the author/funder, who has granted bioRxiv a license to display the preprint in perpetuity. It is made available under a CC-BY 4.0 International license.

Supplementary Figure S2

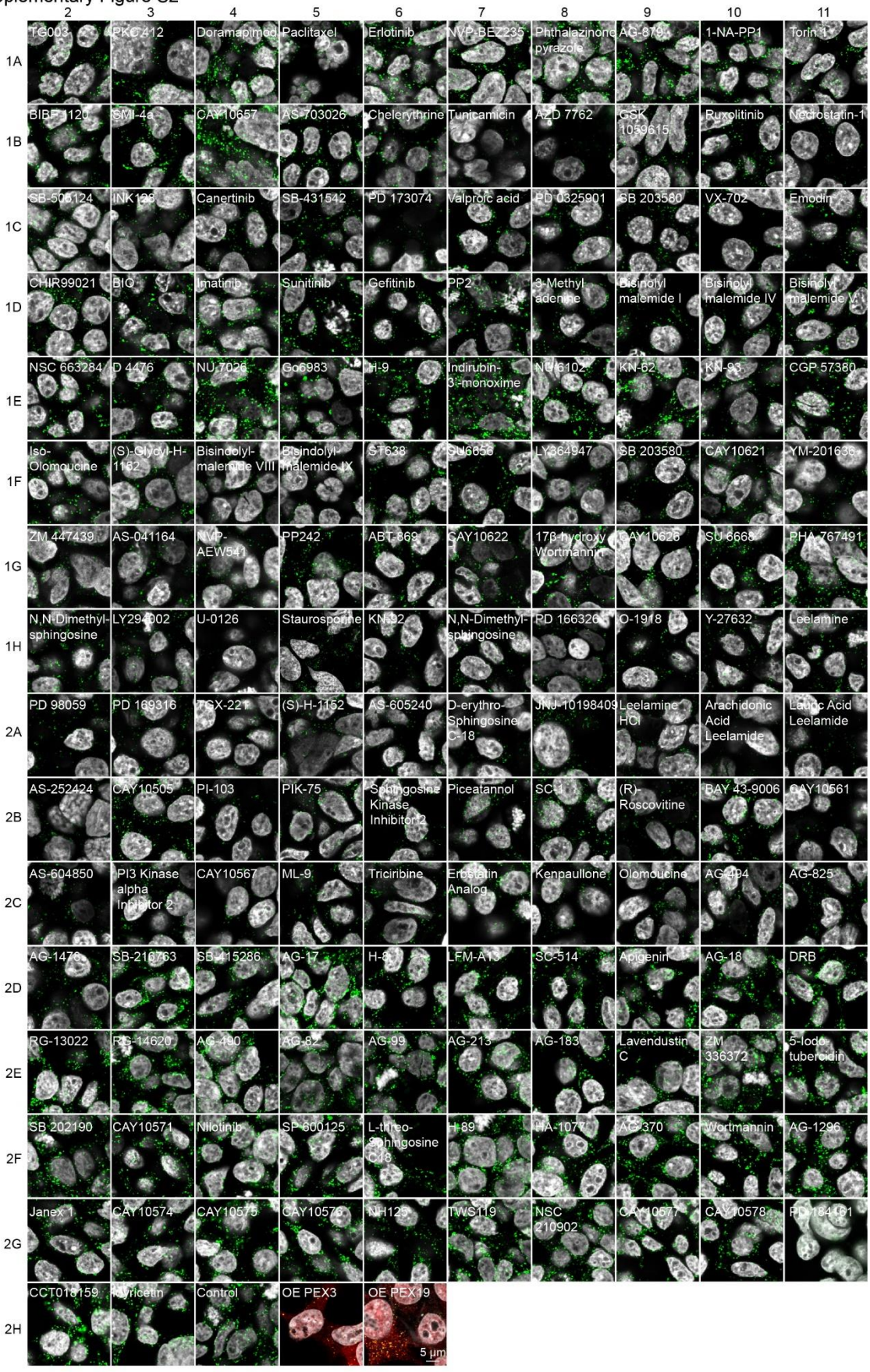

1

bioRxiv preprint doi: https://doi.org/10.1101/2025.01.21.634043; this version posted January 25, 2025. The copyright holder for this preprint (which was not certified by peer review) is the author/funder, who has granted bioRxiv a license to display the preprint in perpetuity. It is made available under a CC-BY 4.0 International license.

Figure S2.

Kinase Inhibitor Screen. Confocal microscopy of the HEK293T CRISPR/Cas9 PMP70-GFP cells incubated for 2 days with 1μM of the indicated small molecule. Note, that endogenous levels of PMP70 vary between treatments as do the numbers of peroxisomes. Scale bar - 5μm.

bioRxiv preprint doi: https://doi.org/10.1101/2025.01.21.634043; this version posted January 25, 2025. The copyright holder for this preprint (which was not certified by peer review) is the author/funder, who has granted bioRxiv a license to display the preprint in perpetuity. It is made available under a CC-BY 4.0 International license.

Supplementary Figure S3

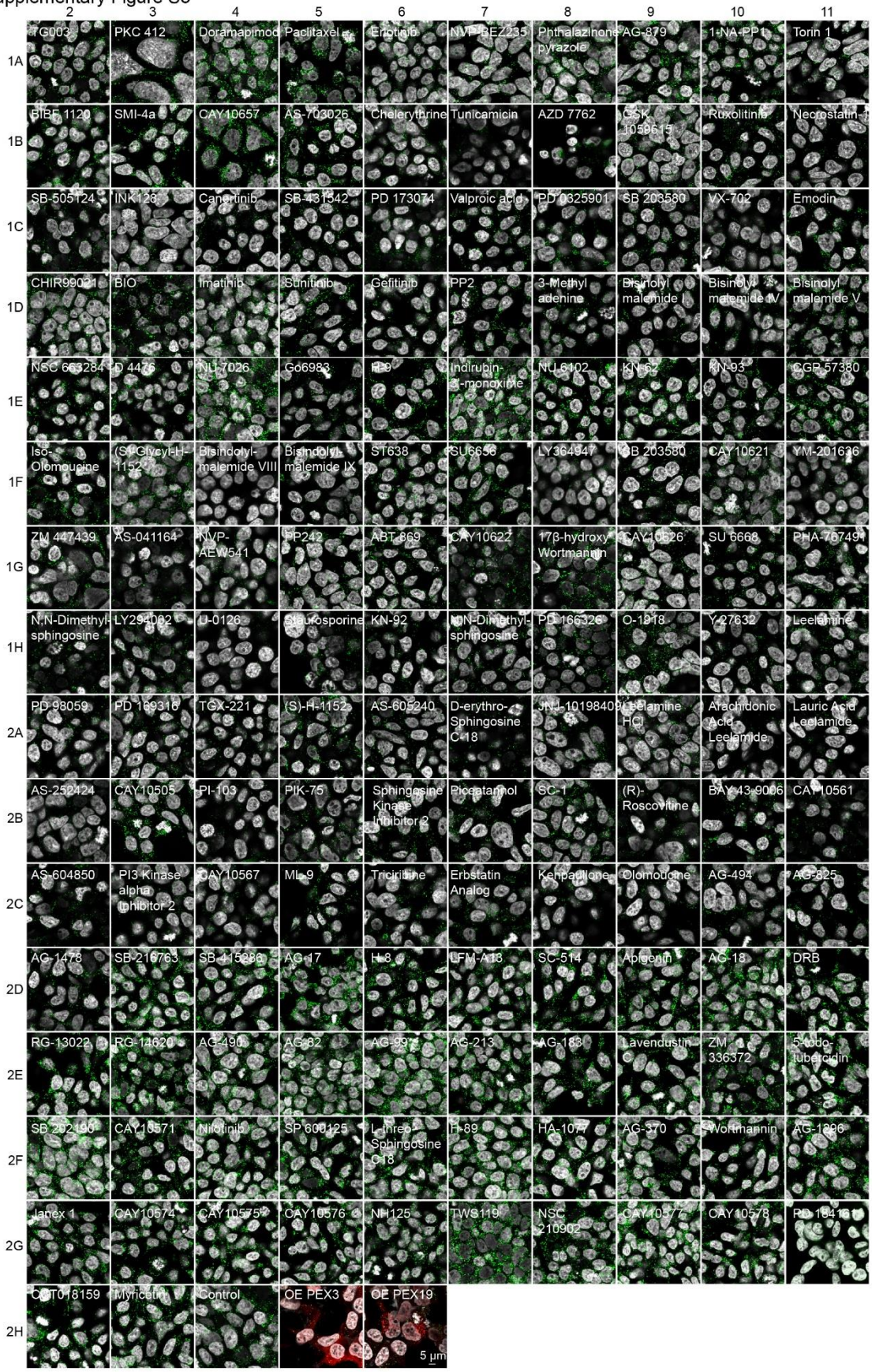

1

bioRxiv preprint doi: https://doi.org/10.1101/2025.01.21.634043; this version posted January 25, 2025. The copyright holder for this preprint (which was not certified by peer review) is the author/funder, who has granted bioRxiv a license to display the preprint in perpetuity. It is made available under a CC-BY 4.0 International license.

Figure S3.

Kinase Inhibitor Screen. Confocal microscopy of the HEK293T CRISPR/Cas9 PMP70-GFP cells incubated for 2 days with 1μM of the indicated small molecule. Note, that endogenous levels of PMP70 vary between treatments as do the numbers of peroxisomes. Scale bar - 5μm.

bioRxiv preprint doi: https://doi.org/10.1101/2025.01.21.634043; this version posted January 25, 2025. The copyright holder for this preprint (which was not certified by peer review) is the author/funder, who has granted bioRxiv a license to display the preprint in perpetuity. It is made available under a CC-BY 4.0 International license.

Supplementary Figure S4

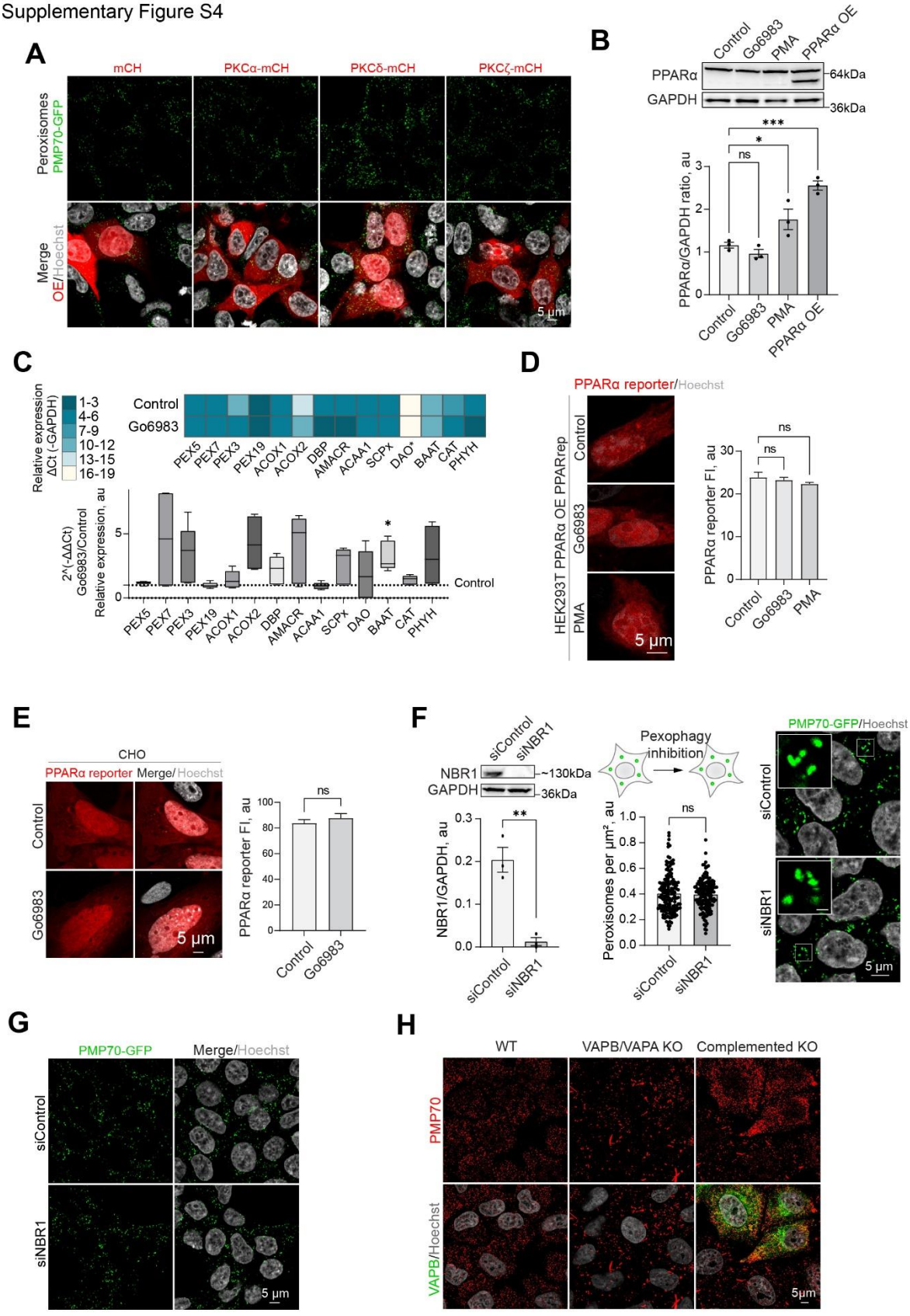

1

bioRxiv preprint doi: https://doi.org/10.1101/2025.01.21.634043; this version posted January 25, 2025. The copyright holder for this preprint (which was not certified by peer review) is the author/funder, who has granted bioRxiv a license to display the preprint in perpetuity. It is made available under a CC-BY 4.0 International license.

Figure S4.

(A) Confocal microscopy of HEK293T CRISPR/Cas9 PMP70-GFP cells overexpressing (OE) PKCα-mCherry, PKCδ-mCherry, or PKCζ-mCherry. Scale bar - 5μm.

(B) Western blot of PPARα in HEK293T cells in control PMA (0.5μM for 1day) and Go6983 (5μM for 2days) conditions. Quantification shows the ratio of PPARα to loading control, mean± SEM , N=3, *** - $p<0.001$, * - $p<0.05$

(C) Quantitative PCR of the peroxisomal genes in HEK293T cells in control and Go6983 5μM conditions (2 day treatment). Quantification shows color coded relative expression levels calculated as a ΔCt (Peroxisomal gene - GAPDH expression reference), and a ratio of Go6983/Contol expression, expressed as $2^{-\Delta\Delta Ct}$, mean± SEM, N=4, * - $p<0.05$.

(D-E) Confocal microscopy of PPAR mCherry reporter in HEK293T cells expressing PPARα (D) and CHO (E) cells in control, Go6983 (5μM for 2days), or PMA conditions (0.5μM for 1day). Nuclei were stained with Hoechst (10μg/ml). Representative images are shown, Scale bar - 5μm. Quantification shows average fluorescence intensity per cell, N=50, **** - $p<0.0001$.

(F-G) Western blot NBR1 and control silencing in HEK293T cells. Quantification shows the NBR1/GAPDH ratio quantified by the lane intensity on the western blot, mean± SEM, N=3, **** - $p<0.0001$. (G) Confocal microscopy of peroxisomes in HEK293T CRISPR/Cas9 PMP70-GFP cells in control silencing or NBR1 silencing conditions. Nuclei were stained with Hoechst (10μg/ml). Representative images are shown, Scale bar - 5μm, inlet - 1μm. Quantification shows the number of peroxisomes per square micron of the cytoplasm in the 2D confocal image, mean± SEM, N=150.

(H) Confocal microscopy of peroxisomes stained with antiPMP70 antibody in WT and VAPB/VAPA KO HeLa cells in control and GFP-VAPB overexpression conditions.

bioRxiv preprint doi: https://doi.org/10.1101/2025.01.21.634043; this version posted January 25, 2025. The copyright holder for this preprint (which was not certified by peer review) is the author/funder, who has granted bioRxiv a license to display the preprint in perpetuity. It is made available under a CC-BY 4.0 International license.

Supplementary Figure S5

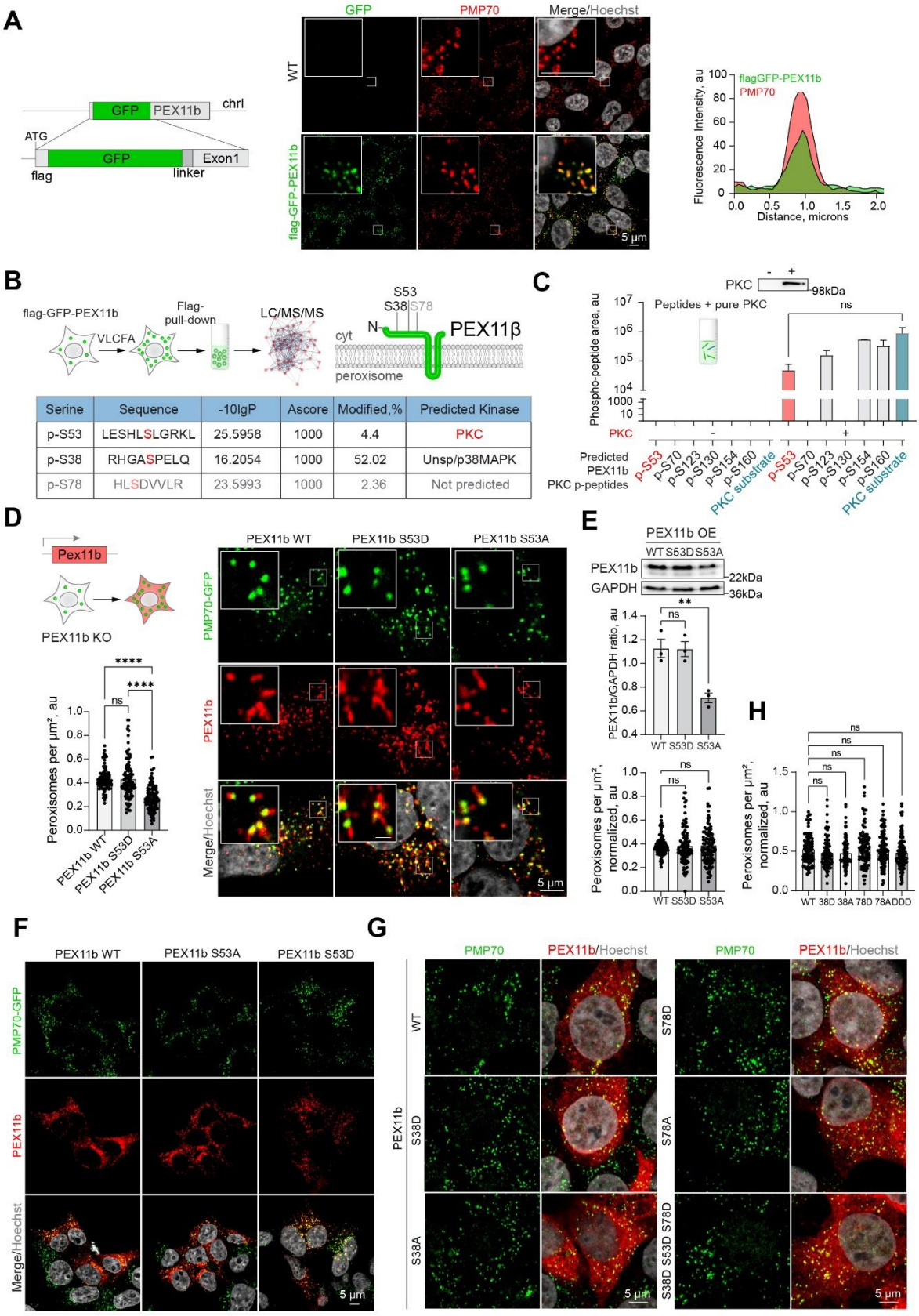

1

Serine	Sequence	-10lgP	Ascore	Modified,%	Predicted Kinase
p-S53	LESHLSLGRKL	25.5958	1000	4.4	PKC
p-S38	RHGASPELQ	16.2054	1000	52.02	Unsp/p38MAPK
p-S78	HLSDVVLR	23.5993	1000	2.36	Not predicted

bioRxiv preprint doi: https://doi.org/10.1101/2025.01.21.634043; this version posted January 25, 2025. The copyright holder for this preprint (which was not certified by peer review) is the author/funder, who has granted bioRxiv a license to display the preprint in perpetuity. It is made available under a CC-BY 4.0 International license.

Figure S5. PKC phosphorylation of PEX11b on S53 is not sufficient to induce peroxisome proliferation

(A) Confocal microscopy of flag-GFP-PEX11b CRISPR/Cas9 tagged HEK293T cells. Peroxisomes were visualized with PMP70 antibody, nuclei were stained with Hoechst (10µg/ml). Scale bar - 5µm, inlet - 1µm. Intensity profile through a single peroxisome is shown. Schematic of CRISPR/Cas9 flag-GFP-PEX11b construction, showing the N-terminal region of genomic DNA corresponding to PEX11b ORF.

(B) Identification of PEX11b phosphorylation by targeted LC-MS/MS analysis, showing the identification of site-specific phosphorylation at residues S38, S53 and S78.

(C) Phosphorylation of pure peptides (a mix of PEX11b peptides predicted to be phosphorylated by PKC, and a PKC-specific substrate peptide) incubated with or without active PKC. Western blot shows PKC in the treated and non-treated samples. Quantification shows the size of the peptide area identified by MS, mean± SEM, N=3, comparison between PKC-specific substrate and the PEX11b peptides.

(D) Confocal microscopy of peroxisomes and PEX11b in HEK293T CRISPR/Cas9 PMP70-GFP PEX11b KO cells overexpressing myc-PEX11b, myc-PEX11b S53A, or myc-PEX11b S53D. Nuclei were stained with Hoechst (10µg/ml). Representative images are shown, Scale bar - 5µm, inlet - 1 µm. Quantification shows the number of peroxisomes per square micron of the cytoplasm in the 2D confocal image, N=100, mean± SEM. ****- $p<0.0001$.

(E) Western blot of myc-PEX11b, myc-PEX11b S53A, or myc-PEX11b S53D, N=3, and corrected quantification showing the number of peroxisomes per square micron, mean± SEM, N=100.

(F) Confocal microscopy of peroxisomes and PEX11b in HEK293T CRISPR/Cas9 PMP70-GFP PEX11b KO cells overexpressing myc-PEX11b or myc-PEX11b S53D. Nuclei were stained with Hoechst (10µg/ml). Representative images are shown, Scale bar - 5µm.

(G-H) Confocal microscopy of peroxisomes and PEX11b in HEK293T overexpressing myc-PEX11b or myc-PEX11b indicated mutants. Nuclei were stained with Hoechst (10µg/ml). Representative images are shown, Scale bar - 5µm. Quantification shows the density of peroxisomes normalized by PEX11b expression level quantified by fluorescence intensity, mean± SEM, N=100.

bioRxiv preprint doi: https://doi.org/10.1101/2025.01.21.634043; this version posted January 25, 2025. The copyright holder for this preprint (which was not certified by peer review) is the author/funder, who has granted bioRxiv a license to display the preprint in perpetuity. It is made available under a CC-BY 4.0 International license.

Supplementary Figure S6

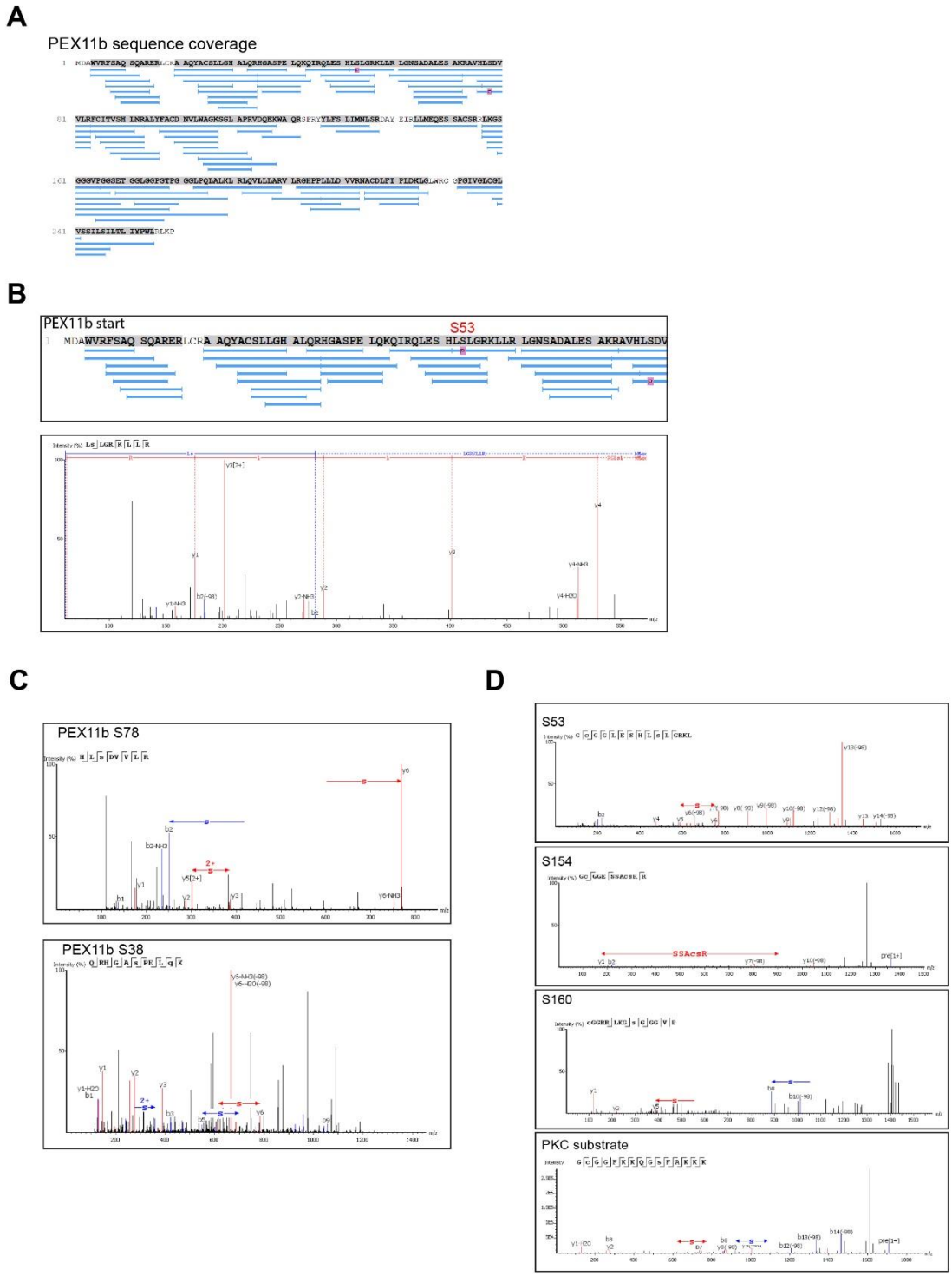

Figure S6.

(A) Peptide coverage of targeted LC-MS/MS analysis of PEX11b

(B) MS/MS spectrum from a targeted, LC-MS/MS analysis of Pex11b peptides, showing the identification of site-specific phosphorylation at residue S53. (Top) PEX11b sequence with identified

bioRxiv preprint doi: https://doi.org/10.1101/2025.01.21.634043; this version posted January 25, 2025. The copyright holder for this preprint (which was not certified by peer review) is the author/funder, who has granted bioRxiv a license to display the preprint in perpetuity. It is made available under a CC-BY 4.0 International license.

peptide sequences (blue lines) and a site-specific phosphorylation. (Bottom) MS/MS spectrum of peptide the sequencing and identification of different -b & -y ions.

(C) MS/MS spectrum from a targeted, LC-MS/MS analysis of Pex11b peptides, showing the identification of site-specific phosphorylation at residue S38, and S78.

(D) Examples of MS/MS spectrums from a peptide competition assay, showing PEX11b phosphor-peptides as well as the PKC-specific phospho-substrate.

bioRxiv preprint doi: https://doi.org/10.1101/2025.01.21.634043; this version posted January 25, 2025. The copyright holder for this preprint (which was not certified by peer review) is the author/funder, who has granted bioRxiv a license to display the preprint in perpetuity. It is made available under a CC-BY 4.0 International license.

Supplementary Figure S7

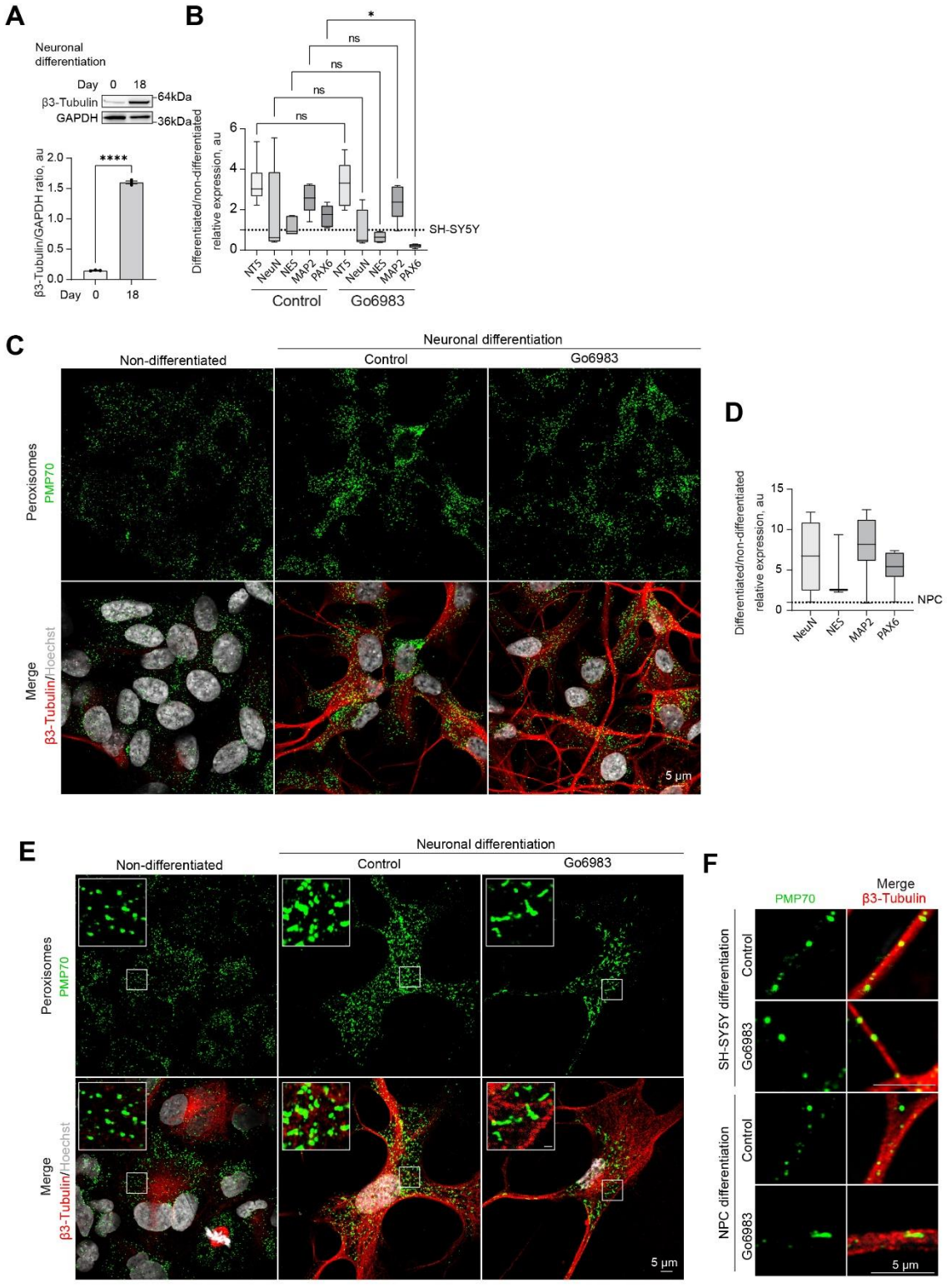

Figure S7.

(A) Western blot of β-3 tubulin in the non-differentiated and 18-day differentiated SH-SY5Y. Quantification shows the ratio of and β-3 tubulin to GAPDH, mean± SEM, N=3, **** - p<0.0001.

bioRxiv preprint doi: https://doi.org/10.1101/2025.01.21.634043; this version posted January 25, 2025. The copyright holder for this preprint (which was not certified by peer review) is the author/funder, who has granted bioRxiv a license to display the preprint in perpetuity. It is made available under a CC-BY 4.0 International license.

(B) Quantitative PCR of the neuronal markers in the 18-day differentiated SH-SY5Y cells in control and Go6983 1μM conditions, Go6983 was added on days 10-18 of the differentiation protocol. Quantification shows the relative expression of differentiated/non-differentiated markers, expressed as $2^{-\Delta\Delta Ct}$, mean± SEM, N=4, * - $p<0.05$.

(C) Confocal microscopy of peroxisomes in the non-differentiated and 18-day differentiated SH-SY5Y cells in control and Go6983 1μM conditions, Go6983 was added on days 10-18 of the differentiation protocol. Peroxisomes were visualized with the PMP70 antibody, nuclei were stained with Hoechst (10μg/ml), and neuronal differentiation was visualized with β-3 tubulin antibody. Representative images are shown, Scale bar - 5μm.

(D) Quantitative PCR of the neuronal markers in the 12-day differentiated NPCs. Quantification shows the relative expression of differentiated/non-differentiated markers, expressed as $2^{-\Delta\Delta Ct}$, mean± SEM.

(E) Confocal microscopy of peroxisomes in the non-differentiated and 12-day differentiated NPCs in control and Go6983 1μM conditions, Go6983 was added on days 1-12 of the differentiation protocol. Peroxisomes were visualized with the PMP70 antibody, nuclei were stained with Hoechst (10μg/ml), and neuronal differentiation was visualized with β-3 tubulin antibody. Representative images are shown, Scale bar - 5μm, inlet - 1μm.

(F) Confocal microscopy of peroxisomes in the neuronal terminals of the 18-day differentiated SH-SY5Y and 12-day differentiated NPCs in control and Go6983 1μM conditions. Peroxisomes were visualized with the PMP70 antibody, and neuronal terminals were visualized with β-3 tubulin antibody. Representative images are shown, Scale bar - 5μm.

bioRxiv preprint doi: https://doi.org/10.1101/2025.01.21.634043; this version posted January 25, 2025. The copyright holder for this preprint (which was not certified by peer review) is the author/funder, who has granted bioRxiv a license to display the preprint in perpetuity. It is made available under a CC-BY 4.0 International license.

Supplementary Figure S8

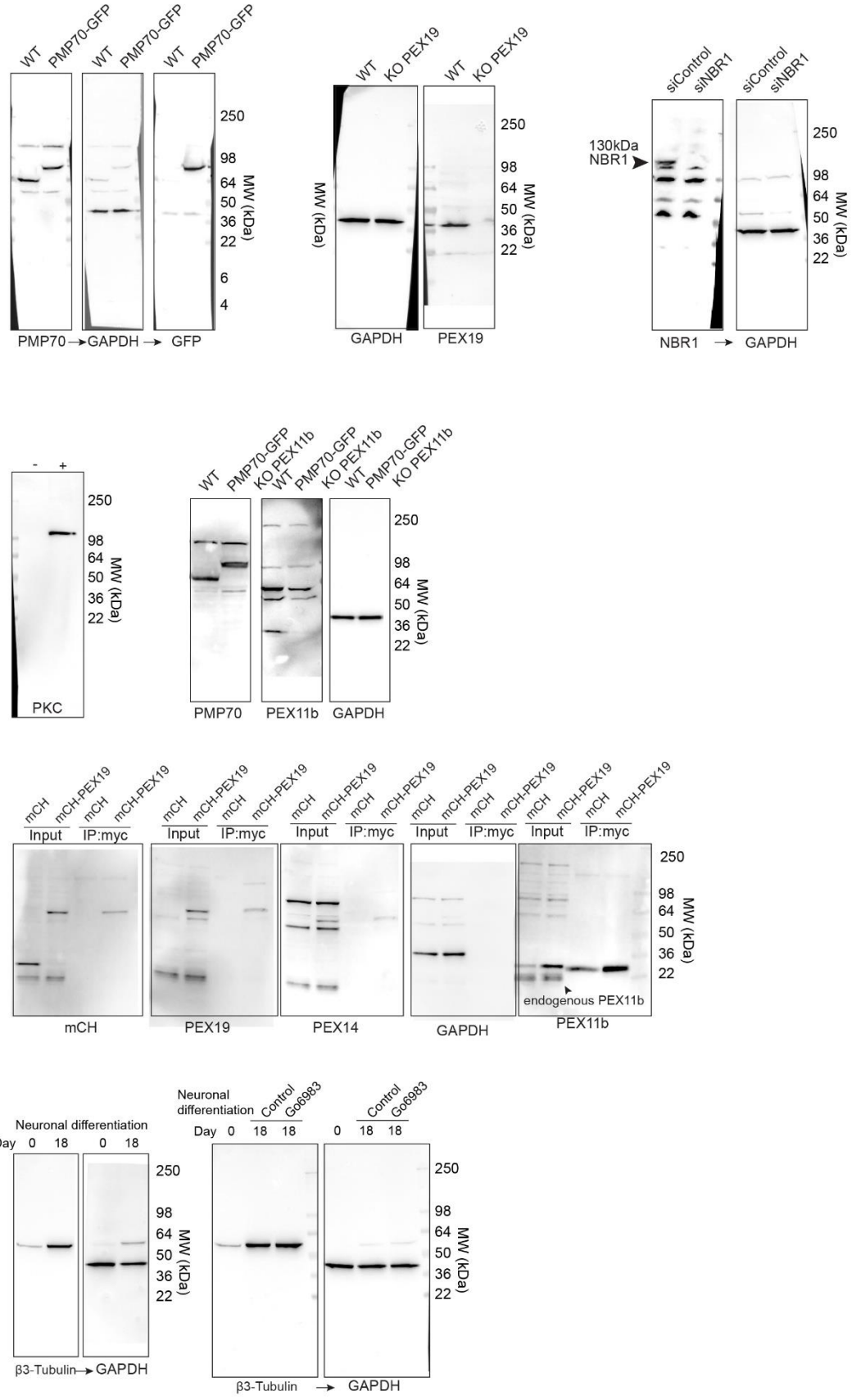

1

bioRxiv preprint doi: https://doi.org/10.1101/2025.01.21.634043; this version posted January 25, 2025. The copyright holder for this preprint (which was not certified by peer review) is the author/funder, who has granted bioRxiv a license to display the preprint in perpetuity. It is made available under a CC-BY 4.0 International license.

Figure S8.

Western blots

Supplementary Figure S9

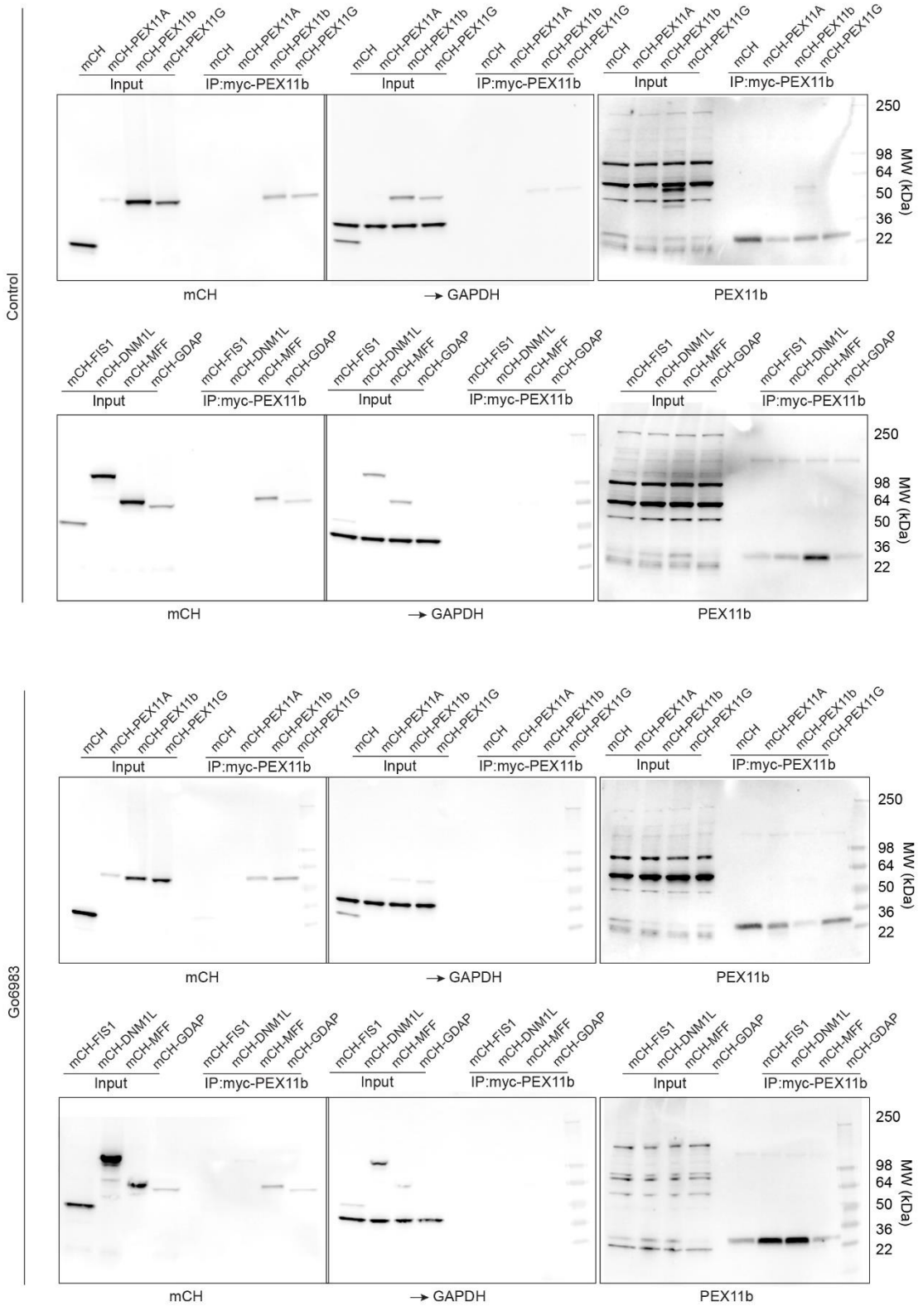

bioRxiv preprint doi: https://doi.org/10.1101/2025.01.21.634043; this version posted January 25, 2025. The copyright holder for this preprint (which was not certified by peer review) is the author/funder, who has granted bioRxiv a license to display the preprint in perpetuity. It is made available under a CC-BY 4.0 International license.

Figure S9.

Western blots

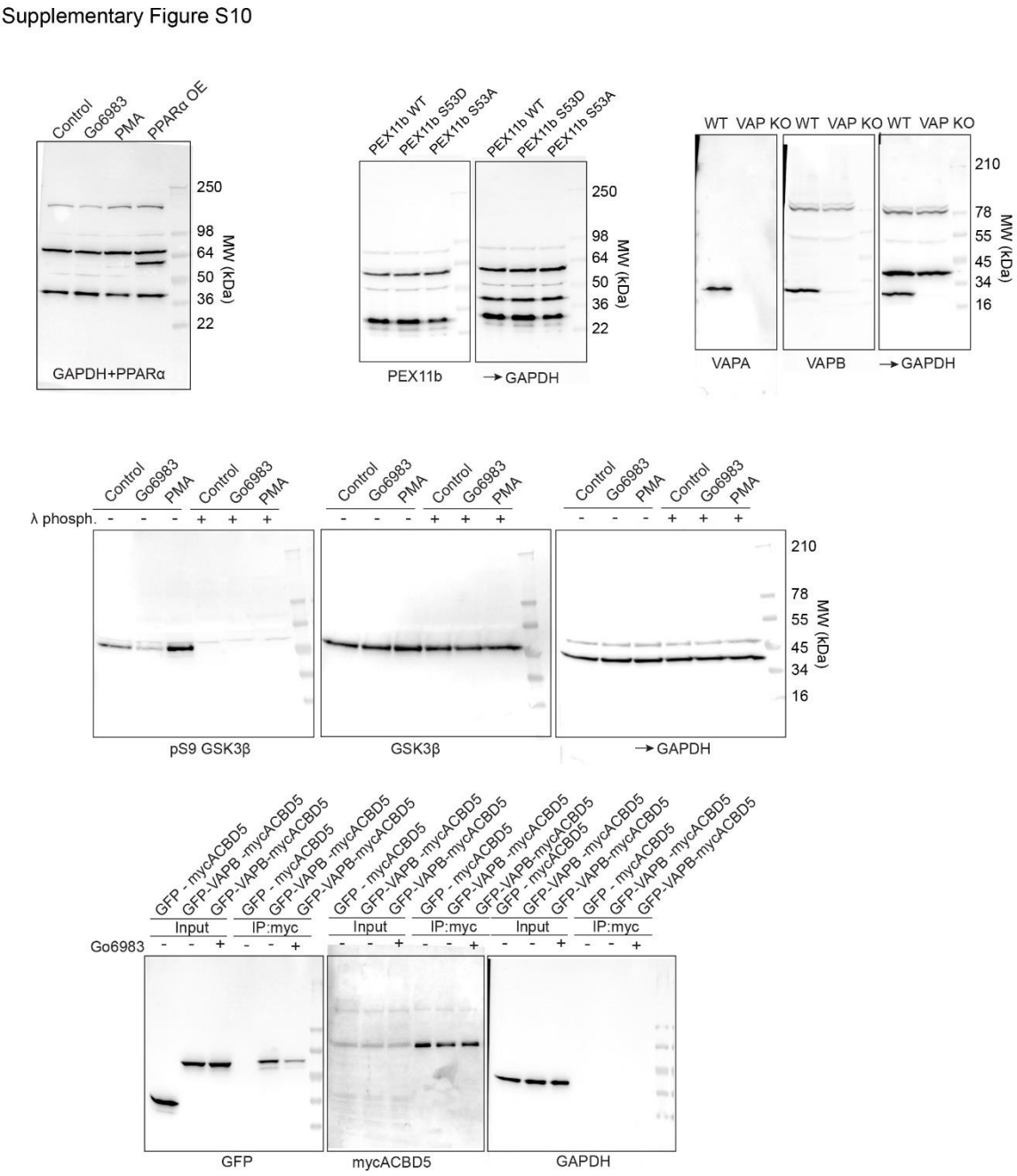

Figure S10.

Western blots

bioRxiv preprint doi: https://doi.org/10.1101/2025.01.21.634043; this version posted January 25, 2025. The copyright holder for this preprint (which was not certified by peer review) is the author/funder, who has granted bioRxiv a license to display the preprint in perpetuity. It is made available under a CC-BY 4.0 International license.

References

1. De Duve, C. & Baudhuin, P. Peroxisomes (microbodies and related particles). *Physiol Rev* **46**, 323-357 (1966).
2. Wanders, R.J. Peroxisomes, lipid metabolism, and peroxisomal disorders. *Mol Genet Metab* **83**, 16-27 (2004).
3. van den Bosch, H., Schutgens, R.B., Wanders, R.J. & Tager, J.M. Biochemistry of peroxisomes. *Annu Rev Biochem* **61**, 157-197 (1992).
4. Keller, G.A., Gould, S., Deluca, M. & Subramani, S. Firefly luciferase is targeted to peroxisomes in mammalian cells. *Proc Natl Acad Sci U S A* **84**, 3264-3268 (1987).
5. Adams, S.T., Jr. & Miller, S.C. Enzymatic promiscuity and the evolution of bioluminescence. *FEBS J* **287**, 1369-1380 (2020).
6. van der Klei, I.J., Harder, W. & Veenhuis, M. Methanol metabolism in a peroxisome-deficient mutant of Hansenula polymorpha: a physiological study. *Arch Microbiol* **156**, 15-23 (1991).
7. van der Klei, I.J., Yurimoto, H., Sakai, Y. & Veenhuis, M. The significance of peroxisomes in methanol metabolism in methylotrophic yeast. *Biochim Biophys Acta* **1763**, 1453-1462 (2006).
8. Jedlitschky, G., Mayatepek, E. & Keppler, D. Peroxisomal leukotriene degradation: biochemical and clinical implications. *Adv Enzyme Regul* **33**, 181-194 (1993).
9. Zaar, K. Light and electron microscopic localization of D-aspartate oxidase in peroxisomes of bovine kidney and liver: an immunocytochemical study. *J Histochem Cytochem* **44**, 1013-1019 (1996).
10. Arnold, G., Liscum, L. & Holtzman, E. Ultrastructural localization of D-amino acid oxidase in microperoxisomes of the rat nervous system. *J Histochem Cytochem* **27**, 735-745 (1979).
11. Van Veldhoven, P.P., Brees, C. & Mannaerts, G.P. D-aspartate oxidase, a peroxisomal enzyme in liver of rat and man. *Biochim Biophys Acta* **1073**, 203-208 (1991).
12. Kunze, M., Pracharoenwattana, I., Smith, S.M. & Hartig, A. A central role for the peroxisomal membrane in glyoxylate cycle function. *Biochim Biophys Acta* **1763**, 1441-1452 (2006).
13. Paudyal, R., Roychoudhry, S. & Lloyd, J. Functions and Remodelling of Plant Peroxisomes. *eLS* (2017).
14. Spiess, G.M. & Zolman, B.K. Peroxisomes as a source of auxin signaling molecules. *Subcell Biochem* **69**, 257-281 (2013).
15. Martin, J.F., Ullan, R.V. & Garcia-Estrada, C. Role of peroxisomes in the biosynthesis and secretion of beta-lactams and other secondary metabolites. *J Ind Microbiol Biotechnol* **39**, 367-382 (2012).
16. Zhang, J. *et al.* A tuberous sclerosis complex signalling node at the peroxisome regulates mTORC1 and autophagy in response to ROS. *Nat Cell Biol* **15**, 1186-1196 (2013).
17. Alexander, A. *et al.* mTOR signaling is regulated by TSC2 at the peroxisome. *Cancer Research* **68**, 2729-2729 (2008).
18. Gough, N.R. Inhibiting mTORC1 at the Peroxisome. *Science Signaling* **6**, ec250-ec250 (2013).
19. Benjamin, D. & Hall, M.N. TSC on the peroxisome controls mTORC1. *Nat Cell Biol* **15**, 1135-1136 (2013).
20. Magalhaes, A.C. *et al.* Peroxisomes are platforms for cytomegalovirus' evasion from the cellular immune response. *Sci Rep* **6**, 26028 (2016).
21. Kataya, A. *et al.* Identification of Arabidopsis Protein Kinases That Harbor Functional Type 1 Peroxisomal Targeting Signals. *Front Cell Dev Biol* **10**, 745883 (2022).
22. Abe, S. *et al.* Localization of Protein Kinase NDR2 to Peroxisomes and Its Role in Ciliogenesis. *J Biol Chem* **292**, 4089-4098 (2017).
23. Chang, C.C. *et al.* Metabolic control of peroxisome abundance. *J Cell Sci* **112 (Pt 10)**, 1579-1590 (1999).
24. Berger, J., Dorninger, F., Forss-Petter, S. & Kunze, M. Peroxisomes in brain development and function. *Biochim Biophys Acta* **1863**, 934-955 (2016).

bioRxiv preprint doi: https://doi.org/10.1101/2025.01.21.634043; this version posted January 25, 2025. The copyright holder for this preprint (which was not certified by peer review) is the author/funder, who has granted bioRxiv a license to display the preprint in perpetuity. It is made available under a CC-BY 4.0 International license.

25. Cai, M. *et al.* Disruption of peroxisome function leads to metabolic stress, mTOR inhibition, and lethality in liver cancer cells. *Cancer Lett* **421**, 82-93 (2018).
26. Charles, K.N. *et al.* Functional Peroxisomes Are Essential for Efficient Cholesterol Sensing and Synthesis. *Front Cell Dev Biol* **8**, 560266 (2020).
27. Di Cara, F. Peroxisomes in host defense. *PLoS Pathog* **16**, e1008636 (2020).
28. Di Cara, F., Sheshachalam, A., Braverman, N.E., Rachubinski, R.A. & Simmonds, A.J. Peroxisome-Mediated Metabolism Is Required for Immune Response to Microbial Infection. *Immunity* **47**, 93-106 e107 (2017).
29. Nath, A.S. *et al.* Modulation of the cell membrane lipid milieu by peroxisomal beta-oxidation induces Rho1 signaling to trigger inflammatory responses. *Cell Rep* **38**, 110433 (2022).
30. Braverman, N.E., D'Agostino, M.D. & Maclean, G.E. Peroxisome biogenesis disorders: Biological, clinical and pathophysiological perspectives. *Dev Disabil Res Rev* **17**, 187-196 (2013).
31. Aubourg, P. & Wanders, R. Peroxisomal disorders. *Handb Clin Neurol* **113**, 1593-1609 (2013).
32. Goldfischer, S. *et al.* Peroxisomal and mitochondrial defects in the cerebro-hepato-renal syndrome. *Science* **182**, 62-64 (1973).
33. Fujiki, Y. Peroxisome biogenesis and peroxisome biogenesis disorders. *FEBS Lett* **476**, 42-46 (2000).
34. Ghaedi, K., Tamura, S., Okumoto, K., Matsuzono, Y. & Fujiki, Y. The peroxin pex3p initiates membrane assembly in peroxisome biogenesis. *Mol Biol Cell* **11**, 2085-2102 (2000).
35. Lazarow, P.B. & Fujiki, Y. Biogenesis of peroxisomes. *Annu Rev Cell Biol* **1**, 489-530 (1985).
36. Sugiura, A., Mattie, S., Prudent, J. & McBride, H.M. Newly born peroxisomes are a hybrid of mitochondrial and ER-derived pre-peroxisomes. *Nature* **542**, 251-254 (2017).
37. Schrader, M., Bonekamp, N.A. & Islinger, M. Fission and proliferation of peroxisomes. *Biochim Biophys Acta* **1822**, 1343-1357 (2012).
38. Schrader, M., Costello, J.L., Godinho, L.F., Azadi, A.S. & Islinger, M. Proliferation and fission of peroxisomes - An update. *Biochim Biophys Acta* **1863**, 971-983 (2016).
39. South, S.T. & Gould, S.J. Peroxisome synthesis in the absence of preexisting peroxisomes. *J Cell Biol* **144**, 255-266 (1999).
40. Tabak, H.F., Braakman, I. & van der Zand, A. Peroxisome formation and maintenance are dependent on the endoplasmic reticulum. *Annu Rev Biochem* **82**, 723-744 (2013).
41. Matsuzono, Y. *et al.* Human PEX19: cDNA cloning by functional complementation, mutation analysis in a patient with Zellweger syndrome, and potential role in peroxisomal membrane assembly. *Proc Natl Acad Sci U S A* **96**, 2116-2121 (1999).
42. Hettema, E.H., Erdmann, R., van der Klei, I. & Veenhuis, M. Evolving models for peroxisome biogenesis. *Curr Opin Cell Biol* **29**, 25-30 (2014).
43. Agrawal, G. & Subramani, S. De novo peroxisome biogenesis: Evolving concepts and conundrums. *Biochim Biophys Acta* **1863**, 892-901 (2016).
44. Hoepfner, D., Schildknegt, D., Braakman, I., Philippsen, P. & Tabak, H.F. Contribution of the endoplasmic reticulum to peroxisome formation. *Cell* **122**, 85-95 (2005).
45. Schrader, M. & Pellegrini, L. The making of a mammalian peroxisome, version 2.0: mitochondria get into the mix. *Cell Death Differ* **24**, 1148-1152 (2017).
46. Honsho, M., Yamashita, S. & Fujiki, Y. Peroxisome homeostasis: Mechanisms of division and selective degradation of peroxisomes in mammals. *Biochim Biophys Acta* **1863**, 984-991 (2016).
47. Matsuzaki, T. & Fujiki, Y. The peroxisomal membrane protein import receptor Pex3p is directly transported to peroxisomes by a novel Pex19p- and Pex16p-dependent pathway. *J Cell Biol* **183**, 1275-1286 (2008).
48. Itoyama, A. *et al.* Mff functions with Pex11pbeta and DLP1 in peroxisomal fission. *Biol Open* **2**, 998-1006 (2013).

bioRxiv preprint doi: https://doi.org/10.1101/2025.01.21.634043; this version posted January 25, 2025. The copyright holder for this preprint (which was not certified by peer review) is the author/funder, who has granted bioRxiv a license to display the preprint in perpetuity. It is made available under a CC-BY 4.0 International license.

49. Gotte, K. *et al.* Pex19p, a farnesylated protein essential for peroxisome biogenesis. *Mol Cell Biol* **18**, 616-628 (1998).
50. Titorenko, V.I. & Rachubinski, R.A. Mutants of the yeast Yarrowia lipolytica defective in protein exit from the endoplasmic reticulum are also defective in peroxisome biogenesis. *Mol Cell Biol* **18**, 2789-2803 (1998).
51. Kim, P.K. & Mullen, R.T. PEX16: a multifaceted regulator of peroxisome biogenesis. *Front Physiol* **4**, 241 (2013).
52. Sacksteder, K.A. *et al.* PEX19 binds multiple peroxisomal membrane proteins, is predominantly cytoplasmic, and is required for peroxisome membrane synthesis. *J Cell Biol* **148**, 931-944 (2000).
53. Schrader, M. *et al.* Expression of PEX11beta mediates peroxisome proliferation in the absence of extracellular stimuli. *J Biol Chem* **273**, 29607-29614 (1998).
54. Li, X. & Gould, S.J. PEX11 promotes peroxisome division independently of peroxisome metabolism. *J Cell Biol* **156**, 643-651 (2002).
55. Orth, T. *et al.* The PEROXIN11 protein family controls peroxisome proliferation in Arabidopsis. *Plant Cell* **19**, 333-350 (2007).
56. Koch, J. *et al.* PEX11 family members are membrane elongation factors that coordinate peroxisome proliferation and maintenance. *J Cell Sci* **123**, 3389-3400 (2010).
57. Schrader, T.A. *et al.* PEX11beta and FIS1 cooperate in peroxisome division independently of mitochondrial fission factor. *J Cell Sci* **135** (2022).
58. Costello, J.L. *et al.* ACBD5 and VAPB mediate membrane associations between peroxisomes and the ER. *J Cell Biol* **216**, 331-342 (2017).
59. Hua, R. *et al.* VAPs and ACBD5 tether peroxisomes to the ER for peroxisome maintenance and lipid homeostasis. *J Cell Biol* **216**, 367-377 (2017).
60. Issemann, I. & Green, S. Activation of a member of the steroid hormone receptor superfamily by peroxisome proliferators. *Nature* **347**, 645-650 (1990).
61. Berger, J. & Moller, D.E. The mechanisms of action of PPARs. *Annu Rev Med* **53**, 409-435 (2002).
62. Abe, I., Okumoto, K., Tamura, S. & Fujiki, Y. Clofibrate-inducible, 28-kDa peroxisomal integral membrane protein is encoded by PEX11. *FEBS Lett* **431**, 468-472 (1998).
63. Chen, C., Li, J., Qin, X. & Wang, W. Peroxisomal Membrane Contact Sites in Mammalian Cells. *Front Cell Dev Biol* **8**, 512 (2020).
64. Kors, S., Kurian, S.M., Costello, J.L. & Schrader, M. Controlling contacts-Molecular mechanisms to regulate organelle membrane tethering. *Bioessays* **44**, e2200151 (2022).
65. Kors, S., Schrader, M. & Costello, J.L. Multiple Ways to Keep FFAT Under Control! *Contact (Thousand Oaks)* **5**, 1-4 (2022).
66. Korotkova, D. *et al.* Fluorescent fatty acid conjugates for live cell imaging of peroxisomes. *Nat Commun* **15**, 4314 (2024).
67. Costello, J.L., Castro, I.G., Schrader, T.A., Islinger, M. & Schrader, M. Peroxisomal ACBD4 interacts with VAPB and promotes ER-peroxisome associations. *Cell Cycle* **16**, 1039-1045 (2017).
68. Kors, S. *et al.* Regulating peroxisome-ER contacts via the ACBD5-VAPB tether by FFAT motif phosphorylation and GSK3beta. *J Cell Biol* **221** (2022).
69. Yamashita, S., Abe, K., Tatemichi, Y. & Fujiki, Y. The membrane peroxin PEX3 induces peroxisome-ubiquitination-linked pexophagy. *Autophagy* **10**, 1549-1564 (2014).
70. Hohfeld, J., Veenhuis, M. & Kunau, W.H. PAS3, a Saccharomyces cerevisiae gene encoding a peroxisomal integral membrane protein essential for peroxisome biogenesis. *J Cell Biol* **114**, 1167-1178 (1991).
71. Azadi, A.S. *et al.* A Functional SMAD2/3 Binding Site in the PEX11beta Promoter Identifies a Role for TGFbeta in Peroxisome Proliferation in Humans. *Front Cell Dev Biol* **8**, 577637 (2020).

bioRxiv preprint doi: https://doi.org/10.1101/2025.01.21.634043; this version posted January 25, 2025. The copyright holder for this preprint (which was not certified by peer review) is the author/funder, who has granted bioRxiv a license to display the preprint in perpetuity. It is made available under a CC BY 4.0 International license.

72. Ma, N. *et al.* Bitopic Inhibition of ATP and Substrate Binding in Ser/Thr Kinases through a Conserved Allosteric Mechanism. *Biochemistry* **57**, 6387-6390 (2018).
73. Herbert, J.M., Augereau, J.M., Gleye, J. & Maffrand, J.P. Chelerythrine is a potent and specific inhibitor of protein kinase C. *Biochem Biophys Res Commun* **172**, 993-999 (1990).
74. Khan, W.A., Dobrowsky, R., el Touny, S. & Hannun, Y.A. Protein kinase C and platelet inhibition by D-erythro-sphingosine: comparison with N,N-dimethylsphingosine and commercial preparation. *Biochem Biophys Res Commun* **172**, 683-691 (1990).
75. Oancea, E. & Meyer, T. Protein kinase C as a molecular machine for decoding calcium and diacylglycerol signals. *Cell* **95**, 307-318 (1998).
76. Azzi, A., Boscoboinik, D. & Hensey, C. The protein kinase C family. *Eur J Biochem* **208**, 547-557 (1992).
77. Sakai, N. *et al.* Direct visualization of the translocation of the gamma-subspecies of protein kinase C in living cells using fusion proteins with green fluorescent protein. *J Cell Biol* **139**, 1465-1476 (1997).
78. Boni, L.T. & Rando, R.R. The nature of protein kinase C activation by physically defined phospholipid vesicles and diacylglycerols. *J Biol Chem* **260**, 10819-10825 (1985).
79. Fujiki, Y., Okumoto, K., Mukai, S., Honsho, M. & Tamura, S. Peroxisome biogenesis in mammalian cells. *Front Physiol* **5**, 307 (2014).
80. Kim, P.K., Mullen, R.T., Schumann, U. & Lippincott-Schwartz, J. The origin and maintenance of mammalian peroxisomes involves a de novo PEX16-dependent pathway from the ER. *J Cell Biol* **173**, 521-532 (2006).
81. Zientara-Rytter, K. & Subramani, S. Autophagic degradation of peroxisomes in mammals. *Biochem Soc Trans* **44**, 431-440 (2016).
82. Sakai, Y., Oku, M., van der Klei, I.J. & Kiel, J.A. Pexophagy: autophagic degradation of peroxisomes. *Biochim Biophys Acta* **1763**, 1767-1775 (2006).
83. Lu, Z. *et al.* Activation of protein kinase C triggers its ubiquitination and degradation. *Mol Cell Biol* **18**, 839-845 (1998).
84. Jean Beltran, P.M. *et al.* Infection-Induced Peroxisome Biogenesis Is a Metabolic Strategy for Herpesvirus Replication. *Cell Host Microbe* **24**, 526-541 e527 (2018).
85. Erdmann, R. & Blobel, G. Giant peroxisomes in oleic acid-induced Saccharomyces cerevisiae lacking the peroxisomal membrane protein Pmp27p. *J Cell Biol* **128**, 509-523 (1995).
86. Shimizu, M., Takeshita, A., Tsukamoto, T., Gonzalez, F.J. & Osumi, T. Tissue-selective, bidirectional regulation of PEX11 alpha and perilipin genes through a common peroxisome proliferator response element. *Mol Cell Biol* **24**, 1313-1323 (2004).
87. Tzeng, J. *et al.* An Ideal PPAR Response Element Bound to and Activated by PPARalpha. *PLoS One* **10**, e0134996 (2015).
88. Amen, T. & Kaganovich, D. Small Molecule Screen Reveals Joint Regulation of Stress Granule Formation and Lipid Droplet Biogenesis. *Front Cell Dev Biol* **8**, 606111 (2020).
89. Deosaran, E. *et al.* NBR1 acts as an autophagy receptor for peroxisomes. *J Cell Sci* **126**, 939-952 (2013).
90. Knoblach, B. & Rachubinski, R.A. Phosphorylation-dependent activation of peroxisome proliferator protein PEX11 controls peroxisome abundance. *J Biol Chem* **285**, 6670-6680 (2010).
91. Joshi, S., Agrawal, G. & Subramani, S. Phosphorylation-dependent Pex11p and Fis1p interaction regulates peroxisome division. *Mol Biol Cell* **23**, 1307-1315 (2012).
92. Thomas, A.S., Krikken, A.M., van der Klei, I.J. & Williams, C.P. Phosphorylation of Pex11p does not regulate peroxisomal fission in the yeast Hansenula polymorpha. *Sci Rep* **5**, 11493 (2015).
93. Blom, N., Sicheritz-Ponten, T., Gupta, R., Gammeltoft, S. & Brunak, S. Prediction of post-translational glycosylation and phosphorylation of proteins from the amino acid sequence. *Proteomics* **4**, 1633-1649 (2004).

bioRxiv preprint doi: https://doi.org/10.1101/2025.01.21.634043; this version posted January 25, 2025. The copyright holder for this preprint (which was not certified by peer review) is the author/funder, who has granted bioRxiv a license to display the preprint in perpetuity. It is made available under a CC-BY 4.0 International license.

94. Blom, N., Gammeltoft, S. & Brunak, S. Sequence and structure-based prediction of eukaryotic protein phosphorylation sites. *J Mol Biol* **294**, 1351-1362 (1999).
95. Kang, J.H. *et al.* A short peptide is a protein kinase C (PKC) alpha-specific substrate. *Proteomics* **8**, 2006-2011 (2008).
96. Bonekamp, N.A. *et al.* Self-interaction of human Pex11pbeta during peroxisomal growth and division. *PLoS One* **8**, e53424 (2013).
97. Dong, R. *et al.* Endosome-ER Contacts Control Actin Nucleation and Retromer Function through VAP-Dependent Regulation of PI4P. *Cell* **166**, 408-423 (2016).
98. Li, Y. *et al.* Protein kinase C controls lysosome biogenesis independently of mTORC1. *Nat Cell Biol* **18**, 1065-1077 (2016).
99. Moore, S.F. *et al.* Dual regulation of glycogen synthase kinase 3 (GSK3)alpha/beta by protein kinase C (PKC)alpha and Akt promotes thrombin-mediated integrin alphaIIbbeta3 activation and granule secretion in platelets. *J Biol Chem* **288**, 3918-3928 (2013).
100. Stambolic, V. & Woodgett, J.R. Mitogen inactivation of glycogen synthase kinase-3 beta in intact cells via serine 9 phosphorylation. *Biochem J* **303 (Pt 3)**, 701-704 (1994).
101. Kikkawa, U., Takai, Y., Minakuchi, R., Inohara, S. & Nishizuka, Y. Calcium-activated, phospholipid-dependent protein kinase from rat brain. Subcellular distribution, purification, and properties. *J Biol Chem* **257**, 13341-13348 (1982).
102. Shipley, M.M., Mangold, C.A. & Szpara, M.L. Differentiation of the SH-SY5Y Human Neuroblastoma Cell Line. *J Vis Exp*, 53193 (2016).
103. Gomes, K.N. *et al.* Deficiency of Pkc1 activity affects glycerol metabolism in Saccharomyces cerevisiae. *FEMS Yeast Res* **5**, 767-776 (2005).
104. Vilella, F., Herrero, E., Torres, J. & de la Torre-Ruiz, M.A. Pkc1 and the upstream elements of the cell integrity pathway in Saccharomyces cerevisiae, Rom2 and Mtl1, are required for cellular responses to oxidative stress. *J Biol Chem* **280**, 9149-9159 (2005).
105. Anastasia, S.D. *et al.* A link between mitotic entry and membrane growth suggests a novel model for cell size control. *J Cell Biol* **197**, 89-104 (2012).
106. Clarke, J., Dephoure, N., Horecka, I., Gygi, S. & Kellogg, D. A conserved signaling network monitors delivery of sphingolipids to the plasma membrane in budding yeast. *Mol Biol Cell* **28**, 2589-2599 (2017).
107. Thai, V. *et al.* Protein Kinase C Controls Binding of Igo/ENSA Proteins to Protein Phosphatase 2A in Budding Yeast. *J Biol Chem* **292**, 4925-4941 (2017).
108. Regala, R.P. *et al.* Atypical protein kinase C iota is an oncogene in human non-small cell lung cancer. *Cancer Res* **65**, 8905-8911 (2005).
109. Larsson, C. Protein kinase C and the regulation of the actin cytoskeleton. *Cell Signal* **18**, 276-284 (2006).
110. Kermorgant, S., Zicha, D. & Parker, P.J. PKC controls HGF-dependent c-Met traffic, signalling and cell migration. *EMBO J* **23**, 3721-3734 (2004).
111. Tabuse, Y. *et al.* Atypical protein kinase C cooperates with PAR-3 to establish embryonic polarity in Caenorhabditis elegans. *Development* **125**, 3607-3614 (1998).
112. Marsland, B.J. & Kopf, M. T-cell fate and function: PKC-theta and beyond. *Trends Immunol* **29**, 179-185 (2008).
113. Alvi, F., Idkowiak-Baldys, J., Baldys, A., Raymond, J.R. & Hannun, Y.A. Regulation of membrane trafficking and endocytosis by protein kinase C: emerging role of the pericentrion, a novel protein kinase C-dependent subset of recycling endosomes. *Cell Mol Life Sci* **64**, 263-270 (2007).
114. Amen, T. & Kaganovich, D. Stress granules sense metabolic stress at the plasma membrane and potentiate recovery by storing active Pkc1. *Sci Signal* **13** (2020).
115. Blanquart, C. *et al.* The protein kinase C signaling pathway regulates a molecular switch between transactivation and transrepression activity of the peroxisome proliferator-activated receptor alpha. *Mol Endocrinol* **18**, 1906-1918 (2004).

bioRxiv preprint doi: https://doi.org/10.1101/2025.01.21.634043; this version posted January 25, 2025. The copyright holder for this preprint (which was not certified by peer review) is the author/funder, who has granted bioRxiv a license to display the preprint in perpetuity. It is made available under a CC-BY 4.0 International license.

116. Iwata, J. *et al.* Excess peroxisomes are degraded by autophagic machinery in mammals. *J Biol Chem* **281**, 4035-4041 (2006).
117. Lewis, S.C., Uchiyama, L.F. & Nunnari, J. ER-mitochondria contacts couple mtDNA synthesis with mitochondrial division in human cells. *Science* **353**, aaf5549 (2016).
118. Steinberg, S.F. Mechanisms for redox-regulation of protein kinase C. *Front Pharmacol* **6**, 128 (2015).
119. Fransen, M. & Lismont, C. Redox Signaling from and to Peroxisomes: Progress, Challenges, and Prospects. *Antioxid Redox Signal* **30**, 95-112 (2019).
120. Konishi, H. *et al.* Activation of protein kinase C by tyrosine phosphorylation in response to H2O2. *Proc Natl Acad Sci U S A* **94**, 11233-11237 (1997).
121. Vargas-Lopes, C. *et al.* Protein kinase C activity regulates D-serine availability in the brain. *J Neurochem* **116**, 281-290 (2011).
122. Mitchell, J. *et al.* Familial amyotrophic lateral sclerosis is associated with a mutation in D-amino acid oxidase. *Proc Natl Acad Sci U S A* **107**, 7556-7561 (2010).
123. Morgan, S. *et al.* A comprehensive analysis of rare genetic variation in amyotrophic lateral sclerosis in the UK. *Brain* **140**, 1611-1618 (2017).
124. Paul, P. & de Belleroche, J. The role of D-amino acids in amyotrophic lateral sclerosis pathogenesis: a review. *Amino Acids* **43**, 1823-1831 (2012).
125. Sasabe, J. *et al.* D-amino acid oxidase controls motoneuron degeneration through D-serine. *Proc Natl Acad Sci U S A* **109**, 627-632 (2012).
126. Brown, F.R., 3rd *et al.* Cerebro-hepato-renal (Zellweger) syndrome and neonatal adrenoleukodystrophy: similarities in phenotype and accumulation of very long chain fatty acids. *Johns Hopkins Med J* **151**, 344-351 (1982).
127. Koivunen, J., Aaltonen, V. & Peltonen, J. Protein kinase C (PKC) family in cancer progression. *Cancer Lett* **235**, 1-10 (2006).
128. Bowling, N. *et al.* Increased protein kinase C activity and expression of Ca2+-sensitive isoforms in the failing human heart. *Circulation* **99**, 384-391 (1999).
129. Palaniyandi, S.S., Sun, L., Ferreira, J.C. & Mochly-Rosen, D. Protein kinase C in heart failure: a therapeutic target? *Cardiovasc Res* **82**, 229-239 (2009).
130. Garrido, J.L., Godoy, J.A., Alvarez, A., Bronfman, M. & Inestrosa, N.C. Protein kinase C inhibits amyloid beta peptide neurotoxicity by acting on members of the Wnt pathway. *FASEB J* **16**, 1982-1984 (2002).
131. Ishii, H. *et al.* Amelioration of vascular dysfunctions in diabetic rats by an oral PKC beta inhibitor. *Science* **272**, 728-731 (1996).
132. Maioli, E. & Valacchi, G. Rottlerin: bases for a possible usage in psoriasis. *Curr Drug Metab* **11**, 425-430 (2010).
133. Alkon, D.L., Sun, M.K. & Nelson, T.J. PKC signaling deficits: a mechanistic hypothesis for the origins of Alzheimer's disease. *Trends Pharmacol Sci* **28**, 51-60 (2007).
134. Amen, T. & Kaganovich, D. Stress granules inhibit fatty acid oxidation by modulating mitochondrial permeability. *Cell Rep* **35**, 109237 (2021).
135. Amen, T. & Kaganovich, D. Quantitative photoconversion analysis of internal molecular dynamics in stress granules and other membraneless organelles in live cells. *STAR Protoc* **1**, 100217 (2020).
136. Wang, H.R. *et al.* Regulation of cell polarity and protrusion formation by targeting RhoA for degradation. *Science* **302**, 1775-1779 (2003).
137. Soh, J.W. & Weinstein, I.B. Roles of specific isoforms of protein kinase C in the transcriptional control of cyclin D1 and related genes. *J Biol Chem* **278**, 34709-34716 (2003).
138. Boehm, J.S. *et al.* Integrative genomic approaches identify IKBKE as a breast cancer oncogene. *Cell* **129**, 1065-1079 (2007).
139. He, X., Saint-Jeannet, J.P., Woodgett, J.R., Varmus, H.E. & Dawid, I.B. Glycogen synthase kinase-3 and dorsoventral patterning in Xenopus embryos. *Nature* **374**, 617-622 (1995).

bioRxiv preprint doi: https://doi.org/10.1101/2025.01.21.634043; this version posted January 25, 2025. The copyright holder for this preprint (which was not certified by peer review) is the author/funder, who has granted bioRxiv a license to display the preprint in perpetuity. It is made available under a CC-BY 4.0 International license.

140. Pan, G. *et al.* Multifaceted regulation of hepatic lipid metabolism by YY1. *Life Sci Alliance* **4** (2021).
141. Anwar, M.U. *et al.* ER-Golgi-localized proteins TMED2 and TMED10 control the formation of plasma membrane lipid nanodomains. *Dev Cell* **57**, 2334-2346 e2338 (2022).
142. Ma, Y. *et al.* Functional analysis of molecular and pharmacological modulators of mitochondrial fatty acid oxidation. *Sci Rep* **10**, 1450 (2020).
143. Wanders, R.J. *et al.* Measurement of peroxisomal fatty acid beta-oxidation in cultured human skin fibroblasts. *J Inherit Metab Dis* **18 Suppl 1**, 113-124 (1995).
144. Tinevez, J.Y. *et al.* TrackMate: An open and extensible platform for single-particle tracking. *Methods* **115**, 80-90 (2017).
145. Metz, K.S. *et al.* Coral: Clear and Customizable Visualization of Human Kinome Data. *Cell Syst* **7**, 347-350 e341 (2018).
146. Manning, G., Whyte, D.B., Martinez, R., Hunter, T. & Sudarsanam, S. The protein kinase complement of the human genome. *Science* **298**, 1912-1934 (2002).